ABSTRACT

Title of Dissertation: SOFT MATERIALS BASED ON VESICLES AND BIOPOLYMERS

JAE-HO LEE, DOCTOR OF PHILOSOPHY, 2006

Directed By: PROFESSOR SRINIVASA R. RAGHAVAN,
DEPARTMENT OF CHEMICAL & BIOMOLECULAR ENGINEERING

Vesicles are hollow spherical structures formed by the self-assembly of amphiphilic molecules in aqueous solution. They are of great interest for applications ranging from drug delivery and controlled release to separations and sensing. However, the limited stability of vesicles to external conditions such as pH, temperature or ionic strength has hampered their applicability. In this dissertation, we explore the integration of vesicles with biopolymers as a route to creating vesicle-bearing soft materials with increased stability. Two specific types of such materials are studied: (a) *vesicle gels*, *where the vesicles are linked into a network by biopolymer chains*; and (b) *vesicle-loaded capsules*, *where the vesicles are embedded in biopolymer-based capsules*. The materials we have developed could be useful for the controlled and targeted release of drugs, cosmetics, and other chemicals.

The first part of this dissertation focuses on **vesicle gels**, obtained by adding a hydrophobically-modified polysaccharide, chitosan (denoted as hm-chitosan) to a solution of surfactant vesicles. The resulting gel shows an elastic rheological response, and is able to hold its own weight upon tube inversion. Small-angle neutron

scattering (SANS) and cryo-transmission electron microscopy (cryo-TEM) are used to confirm the existence of vesicles within the gel. Based on these results, the likely structure in these gels is a network of vesicles connected by hm-chitosan chains, with the hydrophobes on the polymer embedded in vesicle bilayers. The SANS and cryo-TEM data also reveal interesting differences in the morphology of the vesicles at low and high polymer concentrations. In particular, adding a high concentration of polymer to unilamellar vesicles is shown to transform some of these into *bilamellar* (double-bilayered) structures. A similar co-existence of unilamellar and bilamellar vesicles is observed in all eukaryotic cells, but this is the first systematic demonstration of the phenomenon in an *in vitro* formulation.

The final part of this dissertation focuses on **vesicle-loaded capsules**. Capsules are created spontaneously when a solution of a cationic biopolymer is added dropwise into a solution of an anionic biopolymer. The driving force for capsule formation is the electrostatic interaction between the biopolymers at the interface of the drop. We modify the above procedure to create capsules with embedded vesicles. Additionally, to demonstrate the potential use of these capsules in targeted drug delivery, we load them with magnetic nanoparticles, and attach antibodies to the capsule surface. Controlled release experiments are conducted with both the vesicle-bearing capsules and with the vesicle gels. In each case, a model dye encapsulated in the vesicles is shown to release slowly over an extended period of time due to the combination of transport resistances from the vesicle bilayer and the capsule/gel. The results indicate the potential utility of these materials for drug delivery applications.

SOFT MATERIALS BASED ON VESICLES AND BIOPOLYMERS

By

Jae-Ho Lee

Dissertation submitted to the Faculty of the Graduate School of the
University of Maryland, College Park, in partial fulfillment
of the requirements for the degree of
Doctor of Philosophy
2006

Advisory Committee:
Professor Srinivasa R. Raghavan, Dept. of Chemical Engineering, Chair
Professor Nam Sun Wang, Dept. of Chemical Engineering
Professor John P. Fisher, Dept. of Chemical Engineering
Professor Robert M. Briber, Dept. of Materials Science & Engineering
Professor Gregory F. Payne, Center for Biosystems Research
Professor Douglas S. English, Dept. of Chemistry

DEDICATION

To my lovely wife, Sungyeon,
my two adorable daughters, Janice and Danielle,
my mother, and parents-in law in gratitude for their support and encouragement.

ACKNOWLEDGEMENTS

I am pleased and honored to have worked with Professor Srini Raghavan. I would like to thank him deeply from my heart for his advice and support. As the first Ph.D. student of his group I am indebted to him in many ways. With him I have enjoyed my research, tried to develop new ideas, and learned how to write and present. At any moment I felt a lot of energy from him, which, I hope, transferred to me.

I would also like to thank my committee members, especially Dr. Greg Payne. Without his help, I would never have enjoyed my research. I would also like to thank Dr. Doug English and his student, Xiang Wang. I appreciate Dr. Rob Briber's help with the SANS experiments at NIST. I would like to acknowledge great teachers (Dr. Nam Wang, Dr. Mikhail Anisimov, Dr. Kyu-Yong Choi, Dr. John Fisher, and Dr. Panos Dimitrakopoulos) for their deep lectures and boundless knowledge. I would also like to acknowledge Dr. Isaac Koh for helping with the antibody experiments.

I am grateful to my all group colleagues who have positively impacted my graduate experience: Bani Cipriano, Shih-Huang Tung, Tanner Davies, Matt Dowling, Hee-Young Lee, Aimee Ketner, Rakesh Kumar, Korean graduate students and several graduate students in our department for their help. I confess that my graduate life would not be easy without them; they all turned boring things into joyful experiences.

I would also like to extend my gratitude to the Congregation at the Global Mission Church and our cell members for their prayer and support.

I would also like to thank my family for their support. Especially, I thank my wife, Sungyeon, for her countless sacrifices, prayer, love and support.

Last but not least, I thank God for His Love, who guides my life and walks with me and my family through happy and hard times. He turned everything into blessings.

“Now faith is being sure of what we hope for and certain of what we do not see,”(Hebrews 11:1)

TABLE OF CONTENTS

List of Tables

Page

List of Figures

Page

Chapter 1

Introduction And Overview

1.1. Problem Description and Motivation

This dissertation revolves around the theme of *vesicles*. Vesicles are hollow spherical structures formed by the self-assembly of surfactants, lipids, or block copolymers in aqueous solution.[1-3] They have long been a scientific curiosity because of their structural resemblance to primitive biological cells (see Chapter 2 for a detailed description). From a technological standpoint, vesicles have attracted a great deal of interest for applications ranging from drug delivery and controlled release to separations and sensing.[1]

Although the potential of vesicles has been well recognized, especially for drug delivery, this has not translated into a wide range of commercial applications yet.[4] The underlying reason for this is the *limited stability* of vesicles to external perturbations caused by pH, temperature, ionic strength or chemical species. For example, in the context of drug delivery, the sensitivity of vesicles to environmental variables causes drug encapsulated in the vesicles to be released too rapidly, or at undesired sites within a target organism.

A related challenge in drug delivery is the need to deliver toxic drugs directly to a target site and nowhere else. This is particularly important in cancer therapy, where chemotherapeutic drug therapy ends up killing healthy cells along with the tumor cells. A preferred alternative would be to deliver drug specifically to the tumor cells alone, thereby minimizing side effects and maximizing the efficacy of the drug.[5] Towards this end, the idea of attaching tumor-specific ligands or antibodies to vesicles has been widely explored.[6,7] However, here again, the relative fragility of vesicles complicates the antibody attachment step. The underlying reason for these problems with vesicles is that they are self-assembled structures, held by weak physical bonds rather than stronger covalent or ionic bonds.

1.2. Proposed Approach

To overcome the above shortcomings of vesicles, a number of approaches have been investigated. For example, new lipids have been synthesized whose bilayers can be stabilized by polymerization. Synthetic polymers, such as polyethylene glycol (PEG) have been tethered to the bilayers of vesicles, and such "PEGylated vesicles" have been shown to have a longer circulation time in an organism compared to conventional vesicles.[8,9]

In this dissertation, we explore the **integration of polymers with vesicles** as a route to creating new and useful classes of soft materials. We focus on systems where the polymer plays an active role in creating a carrier or matrix for the vesicles. The resulting hybrid structure imparts increased stability to the self-assembled vesicles.

Two specific classes of such materials are investigated, and these are depicted in Figure 1.1 and briefly described below.

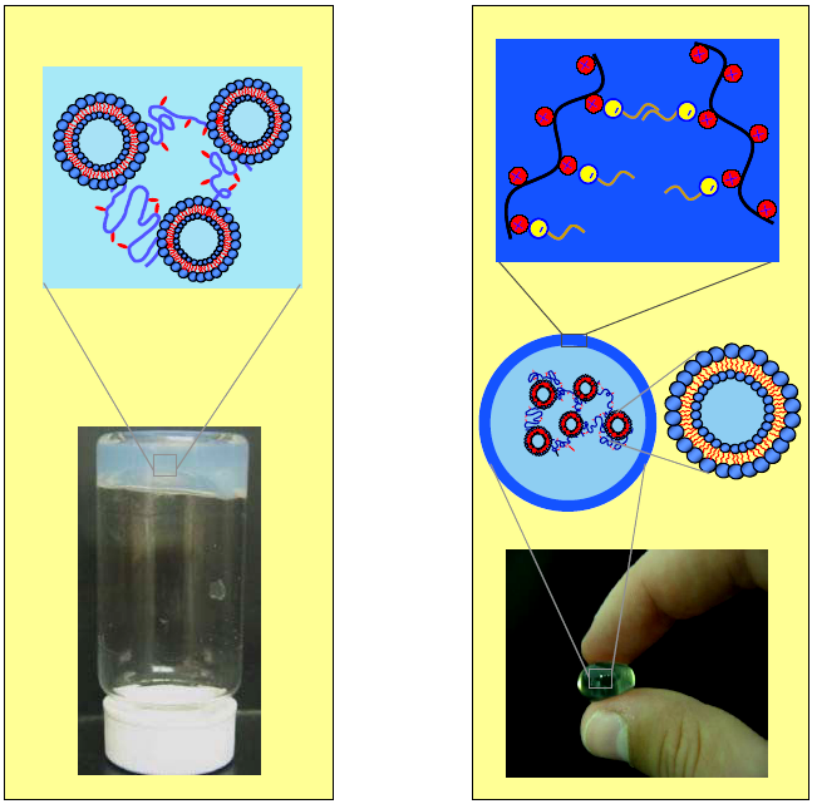

Figure 1.1. Schematic illustrations of the two types of materials investigated in this study. (a) Vesicle gels anchored by biopolymers; (b) Vesicles embedded in biopolymer-based microcapsules.

1.2.1. *Vesicle Gels Anchored by Biopolymers*

The first concept investigated is that of "vesicle gels", which consist of a network of vesicles linked by polymer chains (Figure 1.1a).[10-14] That is, the vesicles form the nodes or junction points in a polymer network, and such a material behaves as a soft, elastic solid (see photograph in Figure 1.1a). The immobilization of vesicles

enhances their stability to external perturbation. To create such a structure, we add a hydrophobically-modified water-soluble polymer (such polymers are referred to as "associating polymers", see Chapter 2) to a vesicle solution. For our work in this area, we have modified the polysaccharide, chitosan, so that it has hydrophobic alkyl tails attached to its backbone. Vesicle gels formed by adding the modified chitosan to surfactant vesicles are studied in Chapter 3. In the course of our investigations, we found that the structure of vesicles in such gels depends on the concentration of polymer relative to that of the vesicles. At high polymer:vesicle ratios, the vesicles transform from unilamellar to bilamellar structures. Studies on this transformation of vesicle structures are the focus of Chapter 4. Finally, controlled release studies from lipid vesicle gels, with a model hydrophilic dye encapsulated in the interior of the vesicles, are described in Chapter 5.

1.2.2. *Vesicles Loaded into Biopolymer Capsules*

The second type of structure investigated is one where vesicles are embedded in capsules formed from biopolymers. Such capsules are created spontaneously when a solution of a cationic biopolymer is added dropwise into a solution of an anionic biopolymer.[15-17] An electrostatic crosslinking occurs at the interface of the drop, leading to an interfacial shell (Figure 1.1c) and this shell protects the contents of the drop from external stimuli. Our studies on chitosan-gelatin capsules loaded with vesicles are described in Chapter 5. Note the container-within-container structure of the final material, as depicted in Figure 1.1c. To demonstrate the potential use of these capsules in targeted drug delivery, they are additionally loaded with magnetic

nanoparticles, and their shells are covalently functionalized with antibodies. Controlled release experiments conducted with the vesicle-bearing capsule show that the combination of transport resistances from the vesicle bilayer and the capsule allow for extended release of encapsulated dye.

1.3. Significance of this Work

The studies described in this dissertation are potentially significant from two different standpoints: (a) *they provide fundamental insight into self-assembly processes, such as in biomolecular systems*; and (b) *the studies provide a foundation for new controlled release concepts that could be important for the pharmaceutical, cosmetic, food, and agrochemical industries*.

First, from a scientific standpoint, the interactions between vesicles and amphiphilic polymers are crucial to the behavior of cell membranes and membrane-bound organelles within a cell. As is well known, every biological membrane consists of a combination of lipids as well as amphiphilic polymers (proteins or polysaccharides) either spanning the membrane or tethered on one side of the membrane. Our studies on a simpler model system of unilamellar vesicles and an amphiphilic biopolymer can still provide insight relevant to biomolecular systems. For example, our findings in Chapter 4 of a polymer-induced transition from unilamellar to bilamellar vesicles may be relevant to the bilamellar structure of intracellular organelles such as the nucleus and mitochondria. Apart from

biomolecular systems, vesicle-polymer interactions are also relevant to the behavior of some consumer products, such as fabric softeners, and cosmetic creams.

Secondly, the vesicle gels and vesicle-loaded capsules described in this dissertation may be useful for controlled release applications. Compared to vesicles alone, the above vesicle-bearing hybrid materials present some benefits. For starters, the stability of vesicles is enhanced by embedding them in the soft biopolymer matrix. Moreover, the presence of an additional transport barrier enables a slower and more extended rate of release for molecules encapsulated in the vesicles. As an added benefit, encapsulation within vesicles may also help in maintaining the bioactivity of drugs and proteins.[4] Vesicles may also be useful as storage depots for hydrophobic drugs that cannot be loaded otherwise into gels or capsules. Finally, we will show that it is relatively easy to confer targeting capabilities (either by magnetic fields or via antibodies) to the capsules, in comparison to the vesicles.

Controlled release applications for vesicle gels could arise either in topical drug delivery or as implantable biomaterials. In addition to drugs, such gels could also be useful in the cosmetic industry as a way to accomplish topical delivery of anti-aging chemicals, for example. Vesicles have also been envisioned as additives in foods, for instance to continuously deliver or replenish ingredients that add flavor. Since a variety of food products, such as yogurt, jellies, ice cream etc. are in a gel-like state, our studies could be relevant in those contexts as well. Applications for the capsules loaded with vesicles are especially likely in targeted drug delivery, for

example, in the targeting of cancerous tumors. To further explore the use of capsules in targeted drug delivery, our group has initiated a collaboration with Dr. Hamid Ghandehari's group at the University of Maryland School of Pharmacy, and these studies will continue in the future.

Chapter 2

Background

In this chapter, we describe some of the basic properties of vesicles, associating polymers, and biopolymers. We then briefly describe the techniques that we will use in this study, specifically, rheology, neutron scattering, and cryo-TEM. The aspects discussed here are of a general nature; literature dealing with more specific aspects are discussed in the Introduction sections of succeeding chapters.

2.1. Vesicles and Liposomes

Vesicles are self-assembled capsules formed in water by lipids, surfactants, or block copolymers.[1,18] The molecules that form vesicles are amphiphilic, with a hydrophilic head (depicted as a blue sphere in Figure 2.1) and hydrophobic tail(s) (shown in red). The shell of the vesicle is a bilayer (*ca*. 2-5 nm in thickness) of these amphiphilic molecules, with the hydrophilic heads on both sides of the bilayer and thereby exposed to water, while the hydrophobic tails inside the bilayer are shielded from water. A vesicle can be considered to form by the folding of amphiphilic bilayers, as shown in Figure 2.1. Vesicles with only a single bilayer (or lamella) are called unilamellar vesicles (ULVs), while vesicles with several concentric bilayers are called multilamellar vesicles (MLVs) and these are also referred to as “onions”.

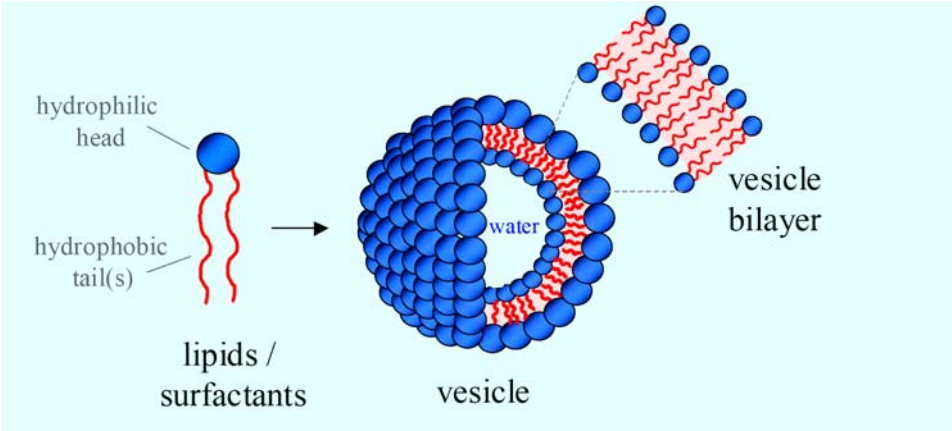

Figure 2.1. The structure of vesicles formed by the self-assembly of amphiphiles. The vesicle is formed by the folding of an amphiphilic bilayer that is about 2-5 nm in thickness.

The folding of bilayers into vesicles tends to occur only when the bilayers are present at low concentration; at high concentrations, bilayers form a lamellar phase.[18] The tendency for bilayers to fold is driven by a desire to minimize contact of the hydrophobes with water at the bilayer ends. Also, the formation of many vesicles from a single extended bilayer sheet increases the entropy of the system. Nevertheless, it is useful to remember that, at equilibrium, the amphiphiles usually exist as a lamellar phase; so, the vesicle state is often of limited stability. In other words, given sufficient time, vesicles will get disrupted and form a dilute lamellar phase. An important exception to this rule exists in the case of mixed surfactants, where vesicles can exist as equilibrium structures.[2]

Vesicles formed from lipids are referred to as “liposomes”. The term lipid usually refers to amphiphiles that have a biological origin and typically, such molecules have two hydrophobic (acyl) tails. Lipid bilayers constitute the membranes

found at the boundary of every living cell as well as many intracellular organelles. The classification of lipids is done based on their headgroup type – for example, phospholipids have a phosphate moiety in their headgroup. Among the phospholipids, the phosphatidylcholines or lecithins are a common variety. Lipids tend to have a very low solubility in water because they have two hydrophobic tails. As a result, an organic solvent is usually employed in preparing lipid vesicles.

The tendency of lipids to form bilayers or vesicles can be rationalized from the geometry of these molecules. Generally speaking, the role of molecular geometry in dictating the self-assembly of amphiphiles can be understood by a term called the critical packing parameter or CPP, which is defined as follows:[19]

$$\mathrm{CPP} = \frac{a_{\mathrm{tail}}}{a_{\mathrm{hg}}} \tag{2.1}$$

where a_{hg} is the effective area of the amphiphile headgroup and a_{tail} is the average area of the amphiphilic tail. Amphiphilic molecules having $a_{\mathrm{tail}} \approx a_{\mathrm{hg}}$, i.e., CPP = 1, tend to assemble into bilayers or vesicles (Figure 2.2). Note that the shape of these molecules resembles that of a cylinder. In contrast, molecules with a larger headgroup area than tail tend to favor curved structures, specifically micelles. A CPP of ⅓ corresponds to spherical micelles while a CPP of ½ corresponds to cylindrical (rodlike or wormlike) micelles.

In addition to lipids (2-tailed amphiphiles), mixtures of single-tailed amphiphiles, one cationic and the other anionic, can also form vesicles.[2] The formation of such "catanionic" vesicles can also be understood via the CPP concept

(Figure 2.2). In this case, each individual surfactant molecule resembles a cone because of the electrostatic repulsion from its headgroup. When mixed together, however, the cationic and anionic headgroups mutually mitigate their repulsive electrostatic effects, leading to a significant reduction in headgroup area. The combination of these molecules thus resembles a cylinder, and consequently leads to vesicle structures. Interestingly, these surfactant vesicles tend to spontaneously form when the two individual surfactants are mixed. Moreover, the vesicles are indefinitely stable, which suggests that they may actually be equilibrium structures.

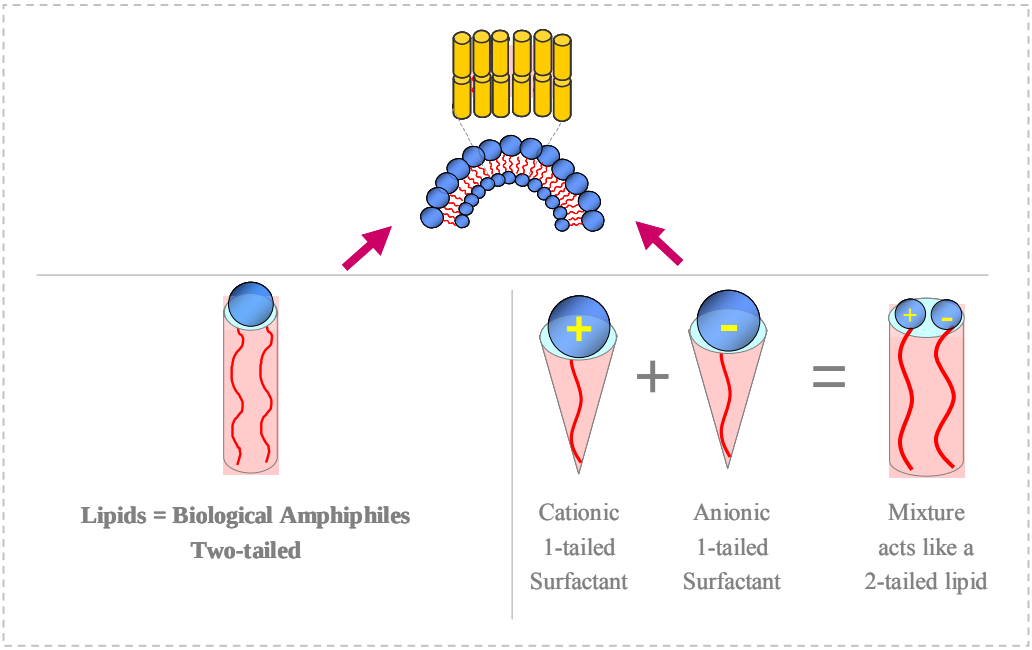

Figure 2.2. Role of geometry in bilayer and vesicle formation. Amphiphiles that have a cylinder-like shape tend to form bilayers. These include lipids (2-tailed biological amphiphiles) as well as mixtures of oppositely-charged single-tailed surfactants.

2.1.1. *Vesicle Preparation from Lipids*

As mentioned, lipids are insoluble in water and at equilibrium they tend to form a lamellar phase. Therefore, preparation of lipid vesicles calls for the use of an organic solvent and some input of energy.[1,20] First, the lipid(s) are dissolved in an organic solvent such as chloroform. Thereafter, the solvent is removed by evaporation to yield a dry lipid film. This film is then hydrated by adding water (or a buffer solution) at a temperature above the gel-to-liquid crystal transition of the lipid (Figure 2.3a). The solution is gently stirred during this process and the result is the formation of large multi-lamellar vesicles (MLVs) in solution. To convert the MLVs to unilamellar vesicles (ULVs), the lipid solution is either sonicated or extruded through a polycarbonate filter of given pore size. Sonication tends to produce small unilamellar vesicles (15 – 50 nm in diameter), whereas extrusion is typically used to produce unilamellar vesicles with a diameter on the order of 100 nm (Figure 2.3a).

While the above methods yield nanometer-sized vesicles, it is also possible to obtain giant unilamellar vesicles (GUVs, or giant vesicles in short) that are several microns in diameter.[21] Giant vesicles can be seen directly by optical microscopy, typically in phase contrast mode. A popular method to form giant vesicles in the size range 5 – 200 μm is by *electroformation* (Figure 2.3b). This involves application of an AC voltage across lipid-coated electrodes spanning a water-filled chamber. In this process, the giant vesicles break off from the lipid film and their size is controlled by the AC voltage and frequency.

.

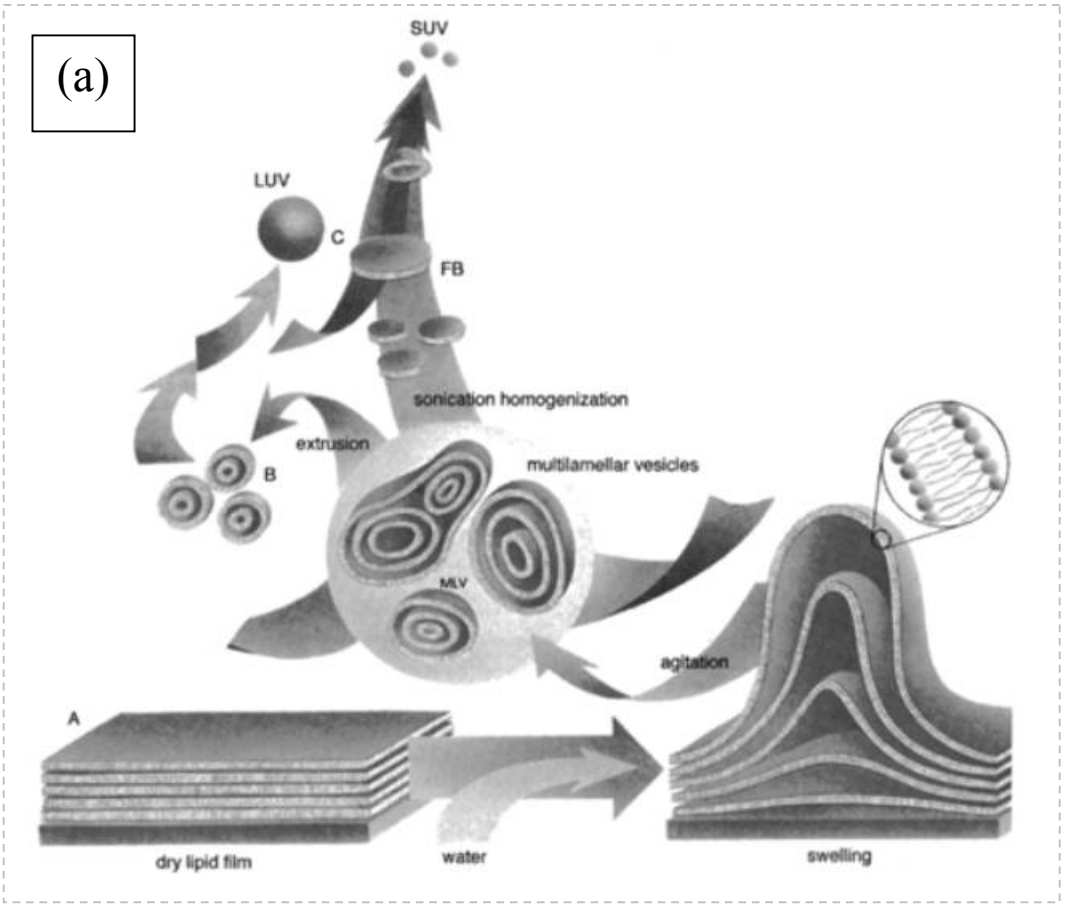

Figure 2.3. Preparation of unilamellar lipid vesicles of various sizes: (a) small or large vesicles (20 nm – 200 nm);[20] (b) giant vesicles by electroformation[21].

2.2. Associating Polymers

The term associating polymer refers to a water-soluble polymer that has an amphiphilic character.[22] Typically, the polymer backbone is hydrophilic, while hydrophobic groups are either present at the ends of the chain (this is called a telechelic structure) or the hydrophobes are tethered by chains to the polymer backbone (this is referred to as a comb-graft structure). Associating polymers have been synthesized by attaching hydrophobes to a range of water-soluble polymers, including polyethylene oxide (PEO) and polyacrylamide (PAAm) as well as to biopolymers such as cellulose and chitosan.[22,23] We will work with chitosan-based associating polymers in this study.

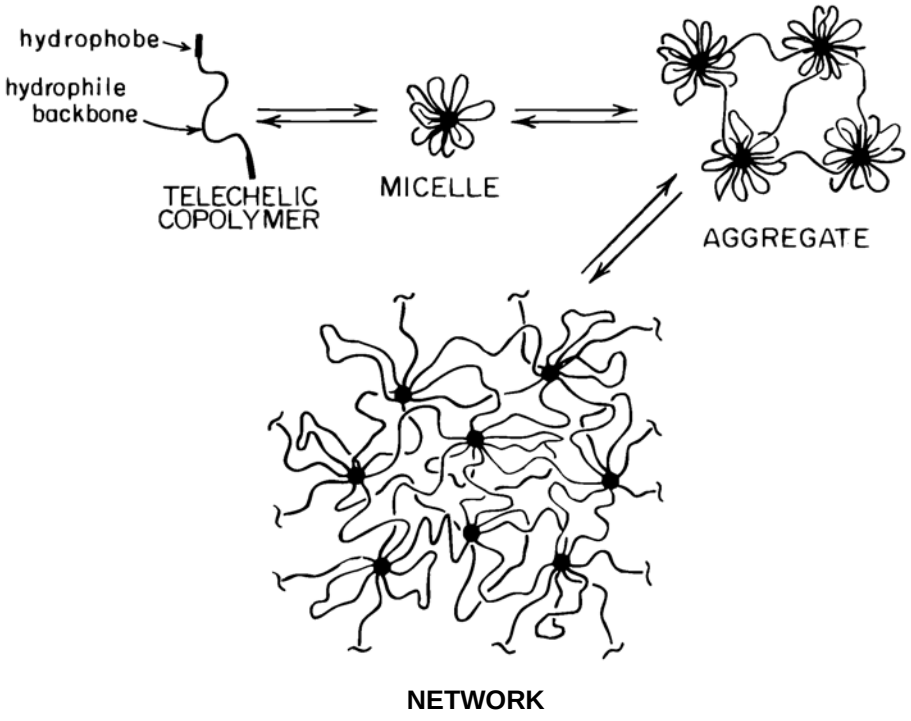

Figure 2.4. Archiecture of a telechelic associating polymer and the structures formed by its self-assembly in aqueous solution (adapted from Ref. 38).

When added to water, hydrophobes on the polymer associate or self-assemble in much the same way as surfactant hydrophobes.[22,24] In analogy to the micelles formed by surfactants, polymer association is believed to result in "flower micelles" (shown in Figure 2.4 for the case of the telechelics), with hydrophobes from many chains present at the center of these micelles. Note that at low polymer concentrations, there is significant *intra*-polymer association, while at higher concentrations, there is a shift to *inter*-polymer associations. Thus, at high polymer concentrations, the flower micelles function as crosslinks in a transient network, thereby enhancing the solution viscosity. For high molecular weights, the polymer will both associate as well as entangle with other chains.

2.3. Biopolymers

Macromolecules of biological origin fall broadly under three classes: polypeptides or proteins; polynucleotides; and polysaccharides.[25] For the purposes of this study, we will focus on polysaccharides. The polysaccharide that is of especial interest to us is chitosan and we describe its properties below in more detail. The common theme with the chosen biopolymers is their ability to render viscosity to water by forming entangled networks or gels.

2.3.1. *Chitosan*

Chitosan is a linear polysaccharide obtained by the deacetylation of chitin.[26] Chitin, in turn, is a natural polysaccharide that constitutes the hard exterior shell of

insects and crustaceans. Among biological polymers, chitin is next only to cellulose in abundance. However, while chitin is insoluble in water, its deacetylated derivative, chitosan, is water-soluble under acidic conditions (pH < 6.5). Under these conditions, the amine groups along the chitosan backbone are ionized and chitosan acts as a cationic polyelectrolyte. Note that chitosan is strictly a copolymer of mostly D-glucosamine (β-(1,4)-2-deoxy-2-amino-D-glucopyranose) sugars and a few of the N-acetyl-D-glucosamine (β-(1,4)-2-deoxy-2-acetamido-D-glucopyranose) sugars from the parent chitin. The structures of these sugars are shown in Figure 2.5.

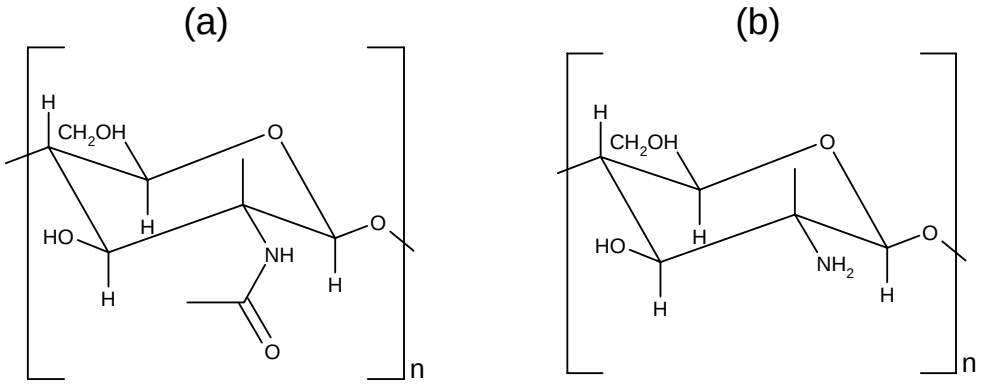

Figure 2.5. Structures of the parent sugars in (a) chitin and (b) chitosan. The N-acetyl-D-glucosamine sugar in chitin is deacetylated to give the D-glucosamine sugar in chitosan.

Current scientific and technological interest in chitosan is motivated by a number of factors.[26] First, chitosan is a biocompatible and biodegradable polymer. It is one of the few cationic biopolymers, and as a result, it can interact with anionic cell membranes. Second, chitosan confers anti-bacterial properties to substrates. As a result, chitosan finds application in tissue regeneration, artificial skin constructs, wound dressings and sutures, drug delivery, antibacterial coatings, and bioseparation

membranes.[26-30] Third, there is an environmental benefit to using chitosan since the parent chitin is usually obtained from food-processing wastes (e.g., crab, shrimp or lobster shells). For these reasons, there is ample interest in chitosan and many researchers have also attempted to modify the parent polymer to confer it unique properties.[30-33] One such modification is to attach hydrophobic groups to chitosan, and this is discussed below.

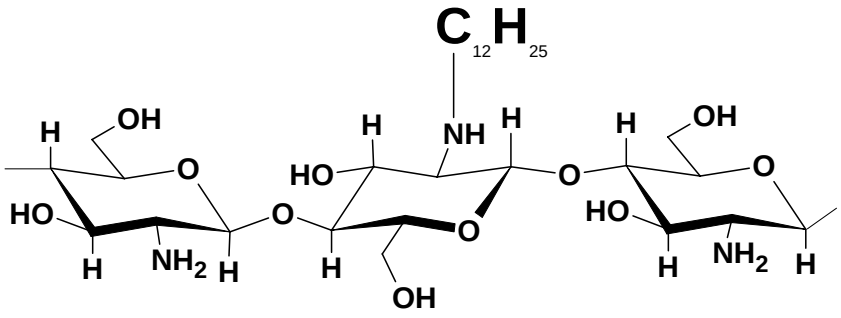

Figure 2.6. Structure of hydrophobically-modified chitosan (hm-chitosan) with C_{12} hydrophobic tails.

2.3.2. *Chitosan Modification*

Chitosan can be modified easily due to its amine groups as well as its primary and secondary hydroxyls. Modifications have been done to improve chitosan solubility in water, to increase its chelating ability, and to modify its antibacterial effect.[23,30,34] Our particular interest is in attaching hydrophobic groups to the chitosan backbone to alter its association behavior in water. The synthesis of hydrophobically-modified chitosan (hm-chitosan) is rather straightforward and can be performed under mild conditions.[23] The procedure involves reacting the chitosan with an *n*-alkyl aldehyde and a typical recipe is described below. In the process, the amine (NH_2)

groups are converted into NH-R groups, where R is the *n*-alkyl moiety. The structure of hm-chitosan containing C_{12} hydrophobic tails is shown in Figure 2.6. Note that this is a comb-graft type of associating polymer.

A typical procedure for synthesizing hm-chitosan with C_{12} tails involves the following steps.[23,34] First, *n*-dodecyl aldehyde is added to an acidic chitosan solution in a water-ethanol mixture, followed by addition of sodium cyanoborohydride. The molar ratio of aldehyde to chitosan monomer(s) is fixed at a certain value (e.g. 2.5%). The reaction yields the hm-chitosan, which is then precipitated by raising the pH and adding ethanol. Next, the precipitate is purified by washing with ethanol followed by deionized water. The final hm-chitosan precipitate is re-dissolved in acetic acid solution and the concentration is recalibrated. This solution tends to be viscous due to associations between the hydrophobes (this is a qualitative indication that the synthesis has been successful). The degree of hydrophobic substitution in the final product can be compared to the value expected from stoichiometry using ^{1}H NMR.

Hydrophobically modified chitosans with *n*-alkyl pendant chains can also be synthesized by alternate routes, e.g., by reacting with alkyl carboxylic acids[35], or alkyl acid anhydrides[36], or alkyl acid chlorides[37]. High substitution levels (> 10%) have been reported via the acid chloride method. These alternate routes are not attempted in the present study.

2.4. Characterization Techniques

2.4.1. *Rheology*

Rheology is formally defined as the study of flow and deformation in materials.[38] Rheological measurements provide important information on soft materials, specifically on the relation between microstructure and macroscopic properties. These measurements are typically performed on a rheometer (Figure 2.7) under steady or dynamic oscillatory shear. Typical geometries used in rheometers are the cone-and-plate, the parallel plate, and the concentric cylinder or Couette.

Figure 2.7. Photograph of the Rheometer RDA-III strain-controlled rheometer being operated in a cone-and-plate geometry.

In ***steady shear rheology***, the sample is subjected to a constant shear-rate $\dot{\gamma}$ (e.g. by applying a continuous rotation at a fixed rate on a rotational instrument), and the response is measured as a shear-stress σ. The ratio of shear-stress σ to shear-rate $\dot{\gamma}$ is the (apparent) viscosity η. A plot of the viscosity vs. shear-rate $\dot{\gamma}$ is called the flow curve of the material.

In ***dynamic or oscillatory rheology***, a sinusoidal strain $\gamma = \gamma_0 \sin(\omega t)$ is imposed on the sample. Here, γ_0 is the strain-amplitude (i.e. the maximum applied deformation) and ω is the frequency of the oscillations. The sample response will be in the form of a sinusoidal stress $\sigma = \sigma_0 \sin(\omega t + \delta)$ which will be shifted by a phase angle δ with respect to the strain waveform. Using trigonometric identities, this stress waveform can be decomposed into two components, one in-phase with the strain and the other out-of-phase by 90°:

$$\sigma = G'\gamma_0 \sin(\omega t) + G''\gamma_0 \cos(\omega t) \qquad (2.2)$$

where G' = **Elastic** or **Storage Modulus**

and G'' = **Viscous** or **Loss Modulus**

The elastic modulus G' is the in-phase component and provides information about the elastic nature of the material. Since elastic behavior implies the storage of deformational energy, this parameter is also called the storage modulus. The viscous modulus G'', on the other hand, is the out-of-phase component and characterizes the viscous nature of the material. Since viscous deformation results in the dissipation of

energy, G'' is also called the loss modulus. For these properties to be meaningful, the dynamic rheological measurements must be made in the "*linear viscoelastic*" (LVE) regime of the sample. This means that the stress must be linearly proportional to the imposed strain (i.e., moduli independent of strain amplitude). In that case, the elastic and viscous moduli are only functions of the frequency of oscillations ω, and are true material functions. A log-log plot of the moduli vs. frequency, i.e. $G'(\omega)$ and $G''(\omega)$, is called the frequency spectrum or *dynamic mechanical spectrum* of the material. Such a plot represents a signature of the material microstructure.

The important advantage of dynamic shear is that it allows us to characterize microstructures without disrupting them in the process. The net deformation imposed on the sample is minimal because the experiments are restricted to small strain amplitudes within the LVE regime of the sample. As a result, the linear viscoelastic moduli reflect the microstructures present in the sample at rest. This is to be contrasted with steady shear, where the material functions are always obtained under flow conditions corresponding to relatively drastic deformations. We can therefore correlate dynamic rheological parameters to static microstructures, and parameters under steady shear to flow-induced changes in microstructure.

2.4.2 *Small-Angle Neutron Scattering (SANS)*

Scattering techniques are invaluable probes of the micro- and nanostructure in soft materials.[39] The basic principle underlying all scattering techniques is that the intensity of scattered radiation is a function of the size, shape, and interactions of the

"particles" present. For aqueous systems, small-angle neutron scattering (SANS) is the technique of choice because contrast between the "particles" and the solvent can be easily achieved by switching H_2O with D_2O. Also, the incident radiation in SANS is composed of neutrons having a wavelength ~ 7 Å, and as a result, SANS is useful in probing size scales on the order of a few nm. SANS experiments require a nuclear reactor to generate neutrons and we are fortunate to have one of the premier SANS facilities in the world close to UMD at NIST in Gaithersburg, MD.

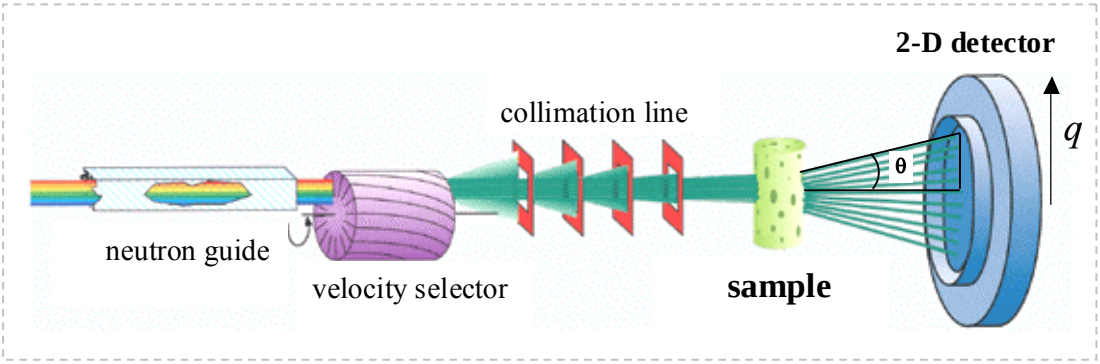

Figure 2.8. Schematic of a SANS experiment.

The basic geometry of a SANS experiment is illustrated in Figure 2.8. Neutrons emitted from a nuclear reactor are selected at a particular wavelength and wavelength spread using a velocity selector, collimated by several lenses, and passed through a sample chamber. The neutrons scattered by the sample are collected on a 2-D detector. This 2-D data is corrected and placed on an absolute scale using calibration standards. It is then converted into a plot of scattered intensity I vs. scattering or wave vector q by spherical averaging. The wave vector q is related to the scattering angle and wavelength by: [39]

$$q = \frac{4\pi}{\lambda}\sin\left(\frac{\theta}{2}\right) \tag{2.3}$$

Here, λ is the wavelength of the incident radiation and θ is the scattering angle. Thus, q can be considered an inverse length scale, with high q corresponding to small structures, and vice versa.

The SANS intensity $I(q)$ from a structured fluid containing n_p particles per unit volume can be expressed in the following manner:[39]

$$I(q) = n_p \cdot P(q) \cdot S(q) \tag{2.4}$$

where $P(q)$ is called the form factor and $S(q)$ the structure factor. $P(q)$ is the scattering that arises from intraparticle interference, which is a function of the particle size and shape. $S(q)$ arises from interparticle interactions and thereby reflects the spatial arrangement of particles in the sample. When the particles are in dilute solution or are non-interacting, the structure factor $S(q) \rightarrow 1$ and the SANS intensity $I(q)$ can then be modeled purely in terms of the form factor $P(q)$. Different expressions exist for the form factor $P(q)$ for various particle geometries. By fitting the appropriate $P(q)$ to the SANS data, one can obtain the characteristic sizes of the particles present.

2.4.3 *Dynamic Light Scattering (DLS)*

Static scattering techniques such as SANS provide important information about the quiescent structure in complex fluids. Dynamic scattering techniques have a complementary role in that they probe structural relaxations and dynamics. In particular, dynamic light scattering (DLS) probes the Brownian motion of particles in the fluid. This method can give a reliable estimate of particle size under certain limiting conditions. In a DLS experiment, the fluctuating intensity of light scattered

from the sample is recorded at a certain angle θ. The fluctuations are then correlated to yield the intensity autocorrelation function $g^{(2)}(q,\tau)$ vs. the correlation time τ.[40]

$$g^{(2)}(q,\tau) = \frac{\langle I(q,t)I(q,t+\tau)\rangle}{\langle I(q,t)^2\rangle} \tag{2.5}$$

Note that in light scattering, the definition of the wave vector is slightly modified as:

$$q = \frac{4\pi n}{\lambda}\sin\left(\frac{\theta}{2}\right) \tag{2.6}$$

where n is the refractive index of the medium. The relevance of q in DLS is that structural relaxations are probed over length scales on the order of q^{-1}.

The measured intensity autocorrelation function $g^{(2)}(q,\ \tau)$ can be converted into an electric field autocorrelation function $g^{(1)}(q,\ \tau)$ through the Siegert relation:

$$g^{(2)}(q,\tau) = 1 + f\left|g^{(1)}(q,\tau)\right|^2 \tag{2.7}$$

Here, f is an adjustable parameter called the coherence factor that depends on the instrument geometry. For a dilute solution of monodisperse spherical particles, the electric-field autocorrelation function is a single exponential whose time decay is determined by the translational diffusion coefficient of the particle D:

$$g^{(1)}(q,\tau) = \exp\left(-Dq^2\tau\right) \tag{2.8}$$

From the measured diffusion coefficient, the particle size can be obtained by the Stokes-Einstein equation:

$$D = \frac{k_B T}{6\pi\eta R_h} \tag{2.9}$$

where k_B is the Boltzmann constant, T the absolute temperature and η the viscosity of the solvent (assumed to be a Newtonian liquid). The size obtained from DLS is the

hydrodynamic radius R_h. The hydrodynamic size is the bare particle size along with any solvation layer.

2.4.4 *Cryo-Transmission Electron Microscopy (Cryo-TEM)*

While scattering techniques provide indirect information about the nanostructure in a sample, an alternate technique that would allow direct visualization of the structure in real space would be extremely useful. Transmission electron microscopy (TEM) can potentially reveal structural detail with sub-nanometer resolution. However, the use of TEM for self-assembled fluids and soft materials is problematic. For imaging under TEM, the solvent must be completely removed, and the process of solvent removal can alter or destroy fragile structures such as micelles and vesicles. Also, to achieve contrast, structures usually have to be stained with heavy metal salts – again, the staining process might degrade the structures present.

The above deficiencies of conventional TEM techniques have led researchers to develop an alternative that is particularly suited for aqueous nanostructured fluids. This technique is called **cryo-TEM**, and it involves the rapid freezing of the aqueous sample such that the water is vitrified instead of forming ice crystals. In the process, the structural details are preserved, and the sample can be imaged under conventional TEM at low electron doses. Sample preparation for cryo-TEM is conducted using a controlled environment vitrification system (CEVS), illustrated in Figure 2.9. In the CEVS, the sample is equilibrated at conditions of controlled temperature and humidity prior to plunge vitrification. First, a drop of the sample is placed on a holey

carbon film supported on a TEM grid. A filter paper is then used to blot the drop, so as to create a thin film of the sample spanning the grid holes. The grid is then plunged into the cryogen, liquid ethane, thereby rapidly vitrifying the sample. Subsequently, the grid has to be transferred to the electron microscope in a dedicated cold stage. Typically, the grid is maintained at –170°C at all times, to ensure that there is no formation of ice crystals nor condensation of atmospheric water.

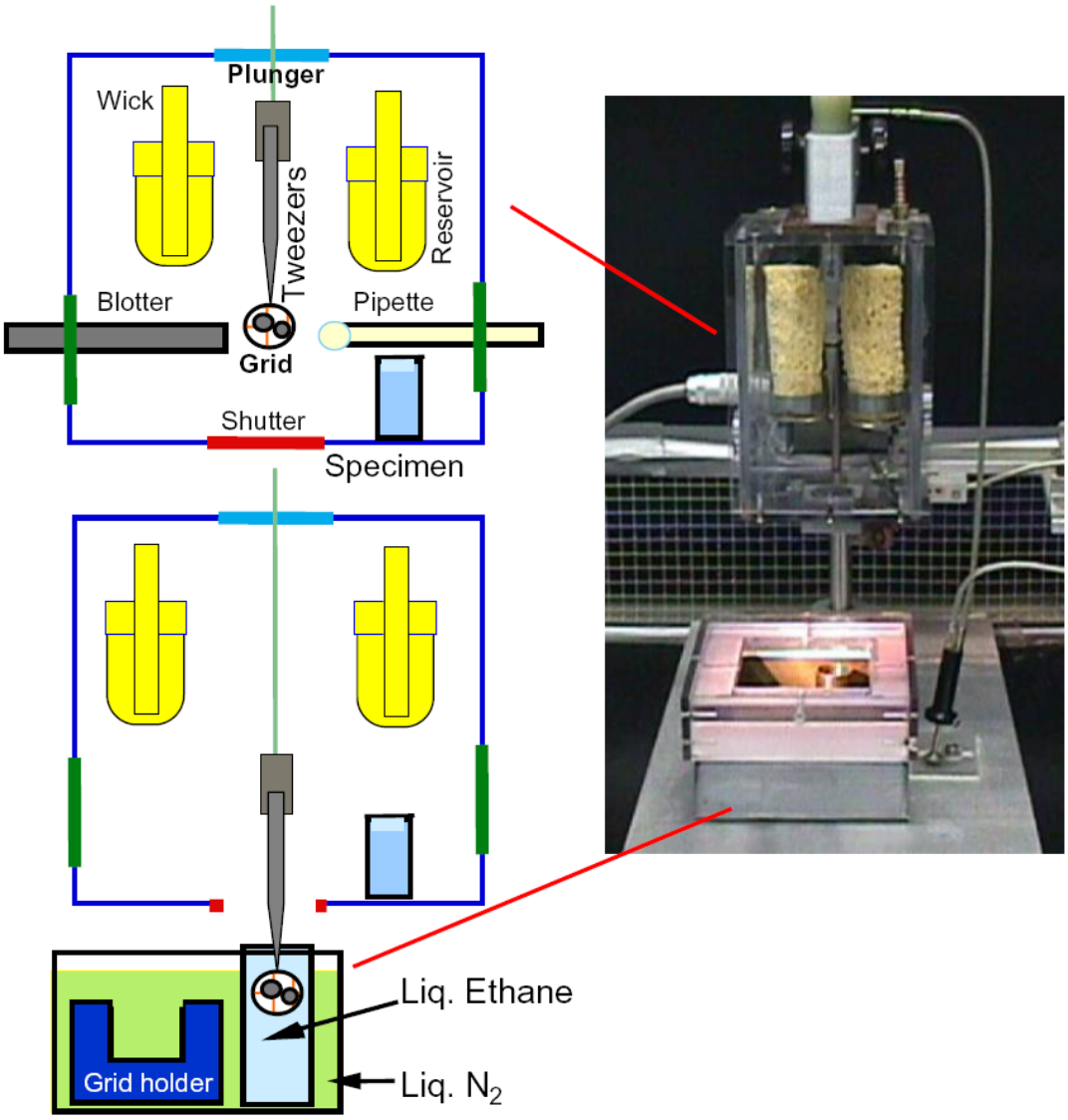

Figure 2.9. Photograph of the controlled environment vitrification system (CEVS) used for sample preparation in cryo-TEM. The schematics on the left show the various steps in the process.

As with any other technique, care has to be taken in interpreting cryo-TEM data. One frequent source of artifacts is that the sample blotting process (used to spread a thin film) involves a substantial amount of shear. This shear may distort the structures present, and one has to take this into account while interpreting images. Despite these artifactual concerns, cryo-TEM has now developed into a powerful tool for directly probing the structures of various complex fluids. A variety of self-assembled structures including micelles, vesicles and liquid crystalline phases have been successfully imaged by cryo-TEM. Also, the use of cryo-TEM in biology has provided unique insights into phenomena such as endocytosis and vesicle fusion.

Chapter 3

Vesicle Gel Networks Anchored by an Associating Biopolymer

The results in this chapter have been published in the following journal article: Jae-Ho Lee, John P. Gustin, Tianhong Chen, Gregory F. Payne and Srinivasa R. Raghavan, "*Vesicle-biopolymer gels: Networks of surfactant vesicles connected by associating biopolymers*." Langmuir 21, 26-33 (**2005**).

3.1. Introduction

In this chapter, we discuss our first study, which is focused on mixtures of vesicles with an associating biopolymer. The biopolymer is the polysaccharide, chitosan, to which we attach *n*-dodecyl tails to convert it into an associating biopolymer. We then show that the addition of this polymer to vesicles results in the formation of "vesicle gels". These gels are studied by a combination of rheological and scattering techniques, and their likely structure is elucidated. As discussed in Chapter 1, our motivation for this work is that the gelation of vesicles can be considered a means of entrapping and stabilizing them within a soft matrix. Vesicle gels could thereby be attractive for controlled release applications.[41]

3.1.1. *Associating Polymer–Vesicle Mixtures*: *Previous Work*

An associating polymer is one with a hydrophilic backbone and pendant hydrophobic groups, as discussed in Chapter 2. While a number of previous studies have investigated mixtures of associating polymers with surfactant micelles, only a few studies have investigated these polymers in conjunction with vesicles. Because associating polymers bear hydrophobes, their interactions with vesicles will be primarily dictated by hydrophobic interactions. If the hydrophobic tails are long enough, they can become embedded in vesicle bilayers and the polymer chain can thereby remain bound to the vesicles through its hydrophobes. The situation is more complicated when the associating polymer itself bears charge (i.e., when it is a *polyelectrolyte*) and the vesicles also bear charge. In the latter case, the net interaction forces will be mediated by a combination of hydrophobic interactions and electrostatic interactions.[42]

Several scenarios can arise as a result of interactions between associating polymers and vesicles. In the simplest scenario, the polymer chains will adsorb on the vesicles through their hydrophobes and act as a stabilizer, i.e., they will impart repulsive interactions to the vesicles.[43] More complicated outcomes can also arise. It is important to note that vesicles are self-assembled entities, and they can thus undergo changes in morphology or shape due to binding of polymer hydrophobes. For example, associating polymers have been known to transform spherical vesicles into faceted (polygon) structures.[43,44] Of particular relevance to the present study is that associating polymers can bridge vesicles to create "vesicle gels".[10-14] These gels

are formed only when there are sufficient numbers of both polymers and vesicles to create a three-dimensional network. A similar network can also be created with cells, rather than vesicles, with associating polymers bound to cell membranes.[11]

So far, studies on vesicle gels have largely been carried out with synthetic associative polymers, obtained typically by attaching hydrophobic moieties to water-soluble synthetic polymers such as polyethylene oxide (PEO) or polyacrylamide (PAAm). In this study, we are interested in creating vesicle gels with an associating *biopolymer*, viz., a hydrophobically-modified chitosan (hm-chitosan). Our use of chitosan is a step towards ensuring the biocompatibility of candidate systems for drug delivery.[27] The synthesis of an hm-chitosan with n-dodecyl tails randomly tethered along its backbone has been described in Section 2.3.2. Earlier investigations with hm-chitosan have focused on its associating properties in water, which has been studied using scattering and rheological techniques. Mixtures of hm-chitosan with surfactant micelles have also been studied, but there have not been any previous studies of hm-chitosans with vesicles.

3.2. Materials and Methods

Chitosan. Chitosan of medium molecular weight (190–310K) and Brookfield viscosity of 286 cps was obtained from Aldrich. The degree of deacetylation was reported to be *ca*. 80% by the manufacturer and this has been verified by NMR. Chitosan is soluble only under acidic conditions, i.e., at a pH < 6.5 and we used 1%

acetic acid to control the pH in chitosan solutions. Chitosan acts as a cationic polyelectrolyte under these conditions.

Hydrophobically-Modified Chitosan (hm-Chitosan). hm-chitosan with *n*-dodecyl tails was synthesized as described in Section 2.3.2 and its structure is shown in Figure 2.7. The molar ratio of aldehyde to that of the chitosan monomer(s) was fixed at 2.5% in this study. The final hm-chitosan precipitate was re-dissolved in 1% acetic acid. As expected, this solution was highly viscous. NMR studies on the hm-chitosan indicated that the degree of hydrophobic substitution was close to that expected from reaction stoichiometry. Similar substitution levels have been reported by others.[45,46]

Vesicles. Surfactant vesicles were prepared by mixing the cationic surfactant, cetyl trimethylammonium tosylate (CTAT), and the anionic surfactant, sodium dodecyl benzene sulfonate (SDBS). The surfactants were purchased from Aldrich and all solutions were made using distilled-deionized water. The phase diagram for CTAT/SDBS mixtures has been reported previously[47] and the water-rich corner of this diagram is redrawn in Figure 3.1. Unilamellar vesicles are present in the two lobes extending from the water corner. The left-hand lobe corresponds to CTAT-rich or cationic vesicles, and our attention was primarily focused on these compositions. The weight ratio of 70/30 CTAT/SDBS in the middle of this lobe was the composition of choice for the majority of our vesicle studies.

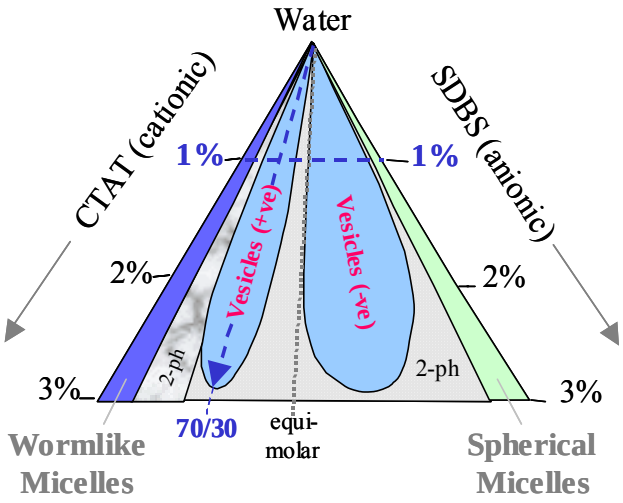

Figure 3.1. Water-rich corner of the CTAT/SDBS/Water ternary phase diagram, redrawn from Ref. 41. All concentrations are expressed in weight%. The focus of this study is on the cationic vesicle phase, with the composition of choice being a 70/30 CTAT/SDBS mixture (dashed arrow).

Sample Preparation and Phase Characterization. Surfactant and polymer mixtures of desired composition were prepared by mixing the corresponding stock solutions. Samples were mildly heated at 50°C for two hours, followed by centrifugation to remove bubbles. The sol-gel phase boundary was evaluated visually by tube inversion (details under Results). For SANS experiments, the samples were prepared in D_2O, obtained from Cambridge Isotopes. The hm-chitosan was vacuum dried before solubilization in D_2O.

Dynamic Light Scattering (DLS). Vesicle solutions were studied at 25°C using a Photocor-FC light scattering instrument with a 5 mW laser light source at 633 nm. The scattering angle was 90° and a logarithmic correlator was used to correlate the intensity. The data yielded the hydrodynamic size of vesicles, as described in Section 2.4.3.[40]

Rheological Studies. Steady and dynamic rheological experiments were performed on a Rheometrics RDA III strain-controlled rheometer. Cone-and-plate geometries (25 mm dia., 0.01 rad cone angle, or 50 mm dia., 0.04 rad cone angle) were used. Dynamic frequency spectra were obtained in the linear viscoelastic regime of the samples, as determined by dynamic strain sweep experiments.

Small-Angle Neutron Scattering (SANS). SANS measurements were made on the NG-3 (30 m) and NG-1 (8 m) beamlines at the National Institute of Standards and Technology (NIST) in Gaithersburg, MD. Samples were studied at 25°C in 2 mm quartz cells. The scattering spectra were corrected and placed on an absolute scale using calibration standards provided by NIST. The final reduced data is plotted as the radially-averaged, absolute intensity I versus the wave vector q.

3.2.1. *SANS Modeling of Vesicles*

We will use SANS as a tool to characterize the sizes of vesicles. The analysis requires fitting the SANS data to a suitable model, which is described below. As discussed in Chapter 2, for a dilute solution of non-interacting vesicles, the structure factor $S(q) \rightarrow 1$, and the SANS intensity $I(q)$ is dictated solely by the form factor $P(q)$. The form factor $P(q)$ for **unilamellar vesicles** of radius R and bilayer thickness t is given by the following expression:[39,48]

$$P(q) = (\Delta\rho)^2 \left\{ \frac{4}{3}\pi R^3 \frac{3J_1(qR)}{qR} - \frac{4}{3}\pi (R+t)^3 \frac{3J_1[q(R+t)]}{q(R+t)} \right\}^2 \qquad (3.1)$$

where ($\Delta\rho$) is the difference in scattering length density between the vesicle bilayer and the solvent. $(\Delta\rho)^2$ is thus a measure of the scattering contrast. $J_1(x)$ is the first-order Bessel function, given by:

$$J_1(x) = \frac{\sin x - x\cos x}{x^2} \tag{3.2}$$

For thin bilayers ($t << R$), or equivalently for large vesicles, $P(q)$ reduces to the following expression:

$$P(q) = \left(\Delta\rho\right)^2 \cdot \left(4\pi R\right)^2 \cdot \frac{t^2}{q^2} \sin^2\left(qR\right) \tag{3.3}$$

Eq 3.3 indicates that for large, non-interacting vesicles, $I(q)$ should show a q^{-2} decay in the low q range. If, the vesicles are polydisperse, the form factor has to be averaged over the vesicle distribution in the following manner: [39,48]

$$P(q) = \int f(R) \cdot P\left(q, R\right)\, dR \tag{3.4}$$

where $P(q, R)$ is the form factor for a vesicle of radius R (eq 1). The polydispersity in vesicle radius $f(R)$ can be accounted for by a Schultz distribution:

$$f(R) = \left(\frac{p+1}{R_0}\right)^{p+1} \frac{R^p}{\Gamma\left(p+1\right)} \exp\left(-\left(p+1\right)\frac{R}{R_0}\right) \tag{3.5}$$

In the above expression, R_0 is the average vesicle radius and p the polydispersity index. The latter is related to the spread of the radius distribution by:

$$\sigma_R = \frac{\Delta R}{R_0} = \frac{1}{\sqrt{p+1}} \tag{3.6}$$

3.3. Results

We performed our initial studies with CTAT/SDBS solutions at a total surfactant concentration of 1 wt.%, indicated in Figure 3.1 by a dashed horizontal line. Samples with various weight ratios of CTAT to SDBS along this line were prepared. When the hm-chitosan was added to samples rich in the anionic surfactant, SDBS, a precipitation occurred, the reasons for which will be clarified in Chapter 5. Our focus here will be restricted to compositions rich in the cationic surfactant, CTAT, i.e., those compositions to the left of the equimolar line in Figure 3.1. Within this composition range, samples in the CTAT-rich corner (CTAT/SDBS weight ratios from 100/0 to about 91/9) consist of rodlike or wormlike micelles. For slightly higher SDBS content (CTAT/SDBS ratios *ca*. 70/30), unilamellar vesicles spontaneously form at equilibrium. Note that these micelles and vesicles both bear a positive charge due to an excess of CTAT. The weight ratio of 70/30 CTAT/SDBS (*ca*. 2:1 molar ratio) falls in the middle of the vesicle lobe and we fixed this composition for the majority of our vesicle studies.

The addition of hm-chitosan has a visible and dramatic effect on CTAT/SDBS vesicles. Consider a 1% mixture of CTAT/SDBS at a 70/30 weight ratio. This sample is located in the vesicle lobe and is a nonviscous, bluish solution, reflecting the presence of unilamellar vesicles (Figure 3.2a). DLS measurements reveal that the vesicle diameter is approximately 120 nm in this sample. When a solution of 0.55% hm-chitosan is added, the sample is instantaneously transformed into an elastic gel that is able to hold its own weight in the vial (Figure 3.2a). Thus, the mixture of the

nonviscous vesicle solution with a small amount of hm-chitosan results in a gel. Interestingly, as seen in Figure 3a, the gel has the same bluish color as does the vesicle solution.

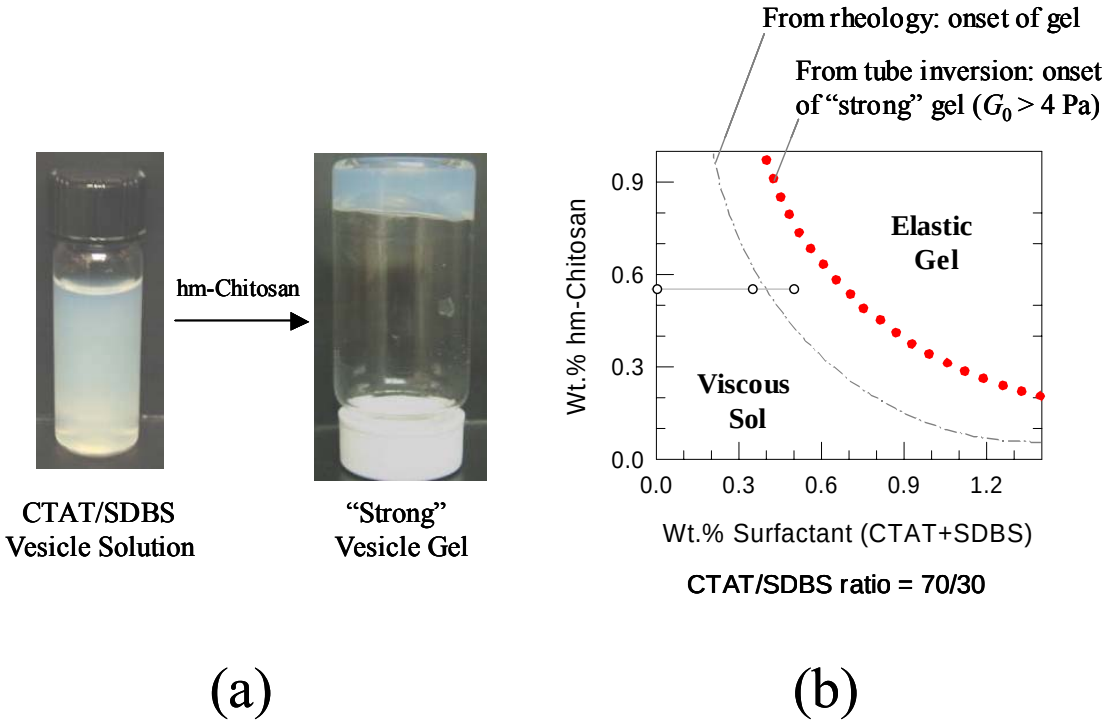

Figure 3.2. (a) Photograph of a CTAT/SDBS vesicle solution before and after addition of hm-chitosan. The polymer transforms the vesicle solution into an elastic gel that is able to hold its own weight in the inverted vial. (b) Phase map of the hm-chitosan/vesicle system showing the sol-gel boundary obtained by tube inversion experiments. This boundary separates samples that are viscous sols from those that are strong elastic gels. An approximate boundary estimated from rheological data, corresponding to the onset of a weak gel (non-zero equilibrium modulus) is also indicated. Dynamic rheological data for the samples marked by unfilled circles are shown in Figure 3.3.

3.3.1. *Phase Behavior and Rheology*

We studied numerous vesicle-polymer mixtures to map out the rheological "phase diagram" shown in Figure 3.2b. This is a plot of hm-chitosan concentration

against total surfactant concentration, with the surfactant ratio fixed at 70/30 CTAT/SDBS. The path of increasing surfactant at this ratio is indicated on the phase diagram (Figure 3.1) by a dashed line. Figure 3.2b shows a sol-gel phase boundary demarcated by tube inversion experiments. Tube inversion is frequently employed in studying gels, and is basically a measure of sample yield stress.[49] Thus, a gel-like sample with sufficient yield stress will be able to hold its own weight in an inverted vial (Figure 3.2a), whereas a viscous sol with a non-existent or low yield stress will drop down. We employed the same amount of sample in identical vials for the tube inversion experiments and observed each sample for several minutes after inversion. As will be shown by rheological measurements, the boundary from tube inversion corresponds to the onset of a "strong" gel, with a modulus around 4 Pa. The boundary represents an inverse relationship between the polymer and the vesicle concentrations. This implies that the onset of a gel requires both a critical vesicle as well as a critical polymer concentration.

The onset of gelation was then studied using dynamic rheology. Figure 3.3 compares the frequency response of four samples with identical hm-chitosan concentrations of 0.55%. The first sample contains no surfactant and the remaining three are vesicle samples (70/30 CTAT/SDBS) with varying surfactant concentrations. The data shows the elastic modulus G' and the viscous modulus G'' as functions of the angular frequency ω. The 0.55% polymer solution is a Newtonian fluid with a viscosity around 35 mPa.s. Its dynamic rheological response reflects its viscous nature (Figure 3.3a) with both the moduli being strong functions of ω and G''

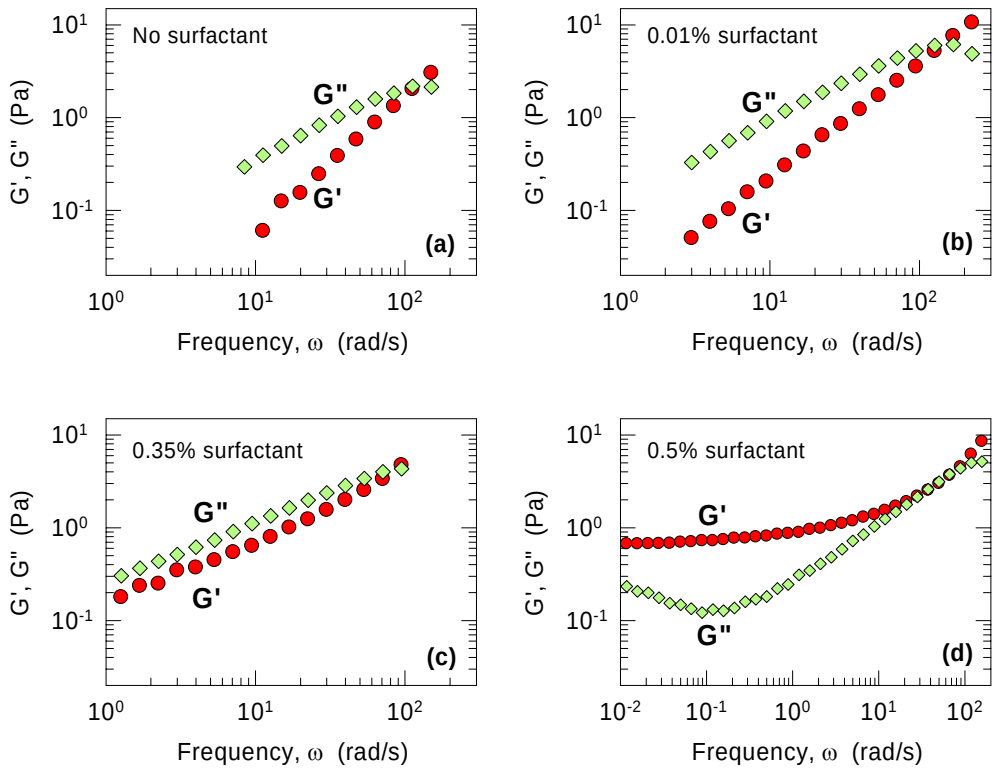

Figure 3.3. Dynamic rheology of vesicle-polymer mixtures as a function of surfactant content. The hm-chitosan is maintained at 0.55% and the CTAT/SDBS ratio is held fixed at 70/30 (within the vesicle region). Data are plotted for (a) polymer with no surfactant; (b) with 0.01% surfactant; (c) with 0.35% surfactant; and (d) with 0.5% surfactant. Samples (a) and (b) are viscous sols, (c) is close to the sol-gel transition, and (d) is a gel, as shown by its frequency-independent elastic modulus G' at low frequencies.

exceeding G' over the entire range of frequencies. At 0.01% surfactant (Figure 3.3b), the rheology is similar to that of the hm-chitosan alone, with a slight increase in the values of both moduli. Increasing the surfactant to 0.35% causes no dramatic changes in the rheology, with G'' still exceeding G' over the frequency range (Figure 3.3c). However, the slopes of G'' and G' on the frequency spectrum become nearly equal, reminiscent of the gel point rheology of a crosslinking polymer.[50] A further increase in surfactant to 0.5% induces a qualitatively different rheological response (Figure 3.3d). In this case, at low frequencies, G' reaches a plateau ($G' = G_0$, the gel modulus,

as $\omega \rightarrow 0$) and its value exceeds that of G''. This indicates *elastic* behavior, and the lack of frequency dependence implies that the sample does not relax, i.e., it has an *infinite* relaxation time. Thus the 0.5% sample satisfies the strict rheological definition of a gel.[38]

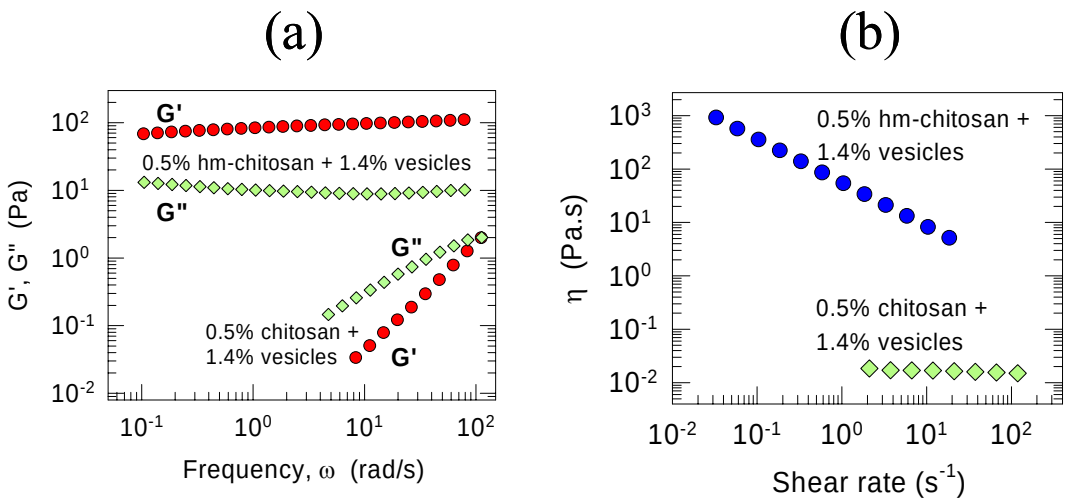

Figure 3.4. Comparison of the native and hydrophobically-modified polymers with regard to their influence on surfactant vesicles. Rheological data under (a) dynamic shear, and (b) steady shear are shown for two samples, each with the same vesicle concentration, i.e., 1.4% CTAT/SDBS at a ratio of 70/30. One sample contains 0.5% of the native chitosan, while the other contains 0.5% hm-chitosan.

Based on visual inspection, the 0.5% surfactant sample (Figure 3.3d) appears to be gel-like; however, it did not pass the tube inversion test. This suggests that the tube inversion boundary in Figure 3.2b is a conservative estimate and corresponds to a higher value of the gel modulus G_0 than at the onset of rheological gelation. The dynamic rheology of a "strong gel" that satisfies the tube inversion test is shown in Figure 3.4a. This sample contains 1.4% surfactant and 0.5% hm-chitosan. In this case, the elastic modulus G' exceeds the viscous modulus G'' over the entire range of frequencies, and both moduli are frequency-independent. Note also that the "strong

gel" in Figure 3.4a has a gel modulus G_0 of about 100 Pa, which is much higher than the G_0 of *ca*. 0.7 Pa for the weak gel in Figure 3.3d. Based on our rheological data, the tube inversion boundary in Figure 3.2b corresponds to a gel modulus of about 4 Pa. We can also draw an approximate boundary corresponding to the onset of gelation from the dynamic rheological data, and this is shown by the dashed curve in Figure 3.2b. The two boundaries have roughly the same shape.

Figure 3.4 also compares the hm-chitosan and the unmodified chitosan in terms of their effect on surfactant vesicles. The dynamic rheology of two samples containing 1.4% surfactant vesicles and 0.5% polymer are contrasted in Figure 3.4a. As discussed above, the hydrophobically modified polymer gives rise to a strong gel that holds its weight under tube inversion. In contrast, the unmodified chitosan merely transforms the bluish vesicle solution into a cloudy and slightly viscous fluid. The cloudiness reflects the onset of phase separation and suggests that the vesicles may be disrupted and/or aggregated into larger structures by the chitosan. The dynamic rheology of the chitosan sample (Figure 3.4a) confirms its viscous behavior, with both moduli being dependent on frequency and the viscous modulus G'' exceeding the elastic modulus G'.

The contrast between the unmodified and hydrophobically-modified chitosan samples is further reinforced by their response under steady-shear (Figure 3.4b), where the viscosity is plotted as a function of shear rate for each case. The chitosan/vesicle mixture is a Newtonian fluid over the range of shear rates, and its viscosity is around 18 mPa.s. On the other hand, the hm-chitosan/vesicle gel strongly

shear-thins and its viscosities are *ca*. four orders of magnitude higher. This response shows the gel-like character of the sample, with the viscosity being infinite in the limit of zero shear rate. Figures 3.4a and 3.4b show that a gel is formed only when the chitosan is hydrophobically-modified.

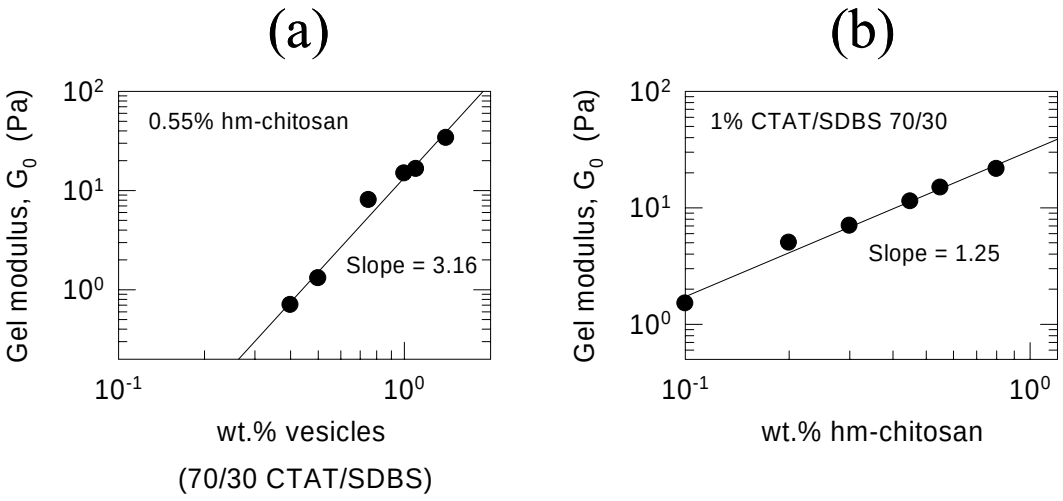

Figure 3.5. Gel modulus G_0 of vesicle gels formed by adding hm-chitosan to CTAT/SDBS mixtures: (a) as a function of vesicle concentration at a constant hm-chitosan concentration of 0.55%; (b) as a function of polymer concentration at a constant vesicle concentration of 1%.

We have studied the rheology of vesicle-polymer gels as a function of polymer and vesicle concentrations. In Figure 3.5a, the hm-chitosan is maintained at 0.55% and the gel modulus G_0 is plotted against vesicle concentration (i.e., total surfactant concentration at a CTAT/SDBS ratio of 70/30). Note that we tabulate G_0 only for gels, i.e., for samples that show a low-frequency plateau in the elastic modulus G'. We find that G_0 sharply increases with vesicle concentration, the approximate relationship being $G_0 \sim c_{\text{ves}}^3$ (the best-fit line through the log-log plot in Figure 3.5a has a slope of 3.16). In a different set of experiments, the vesicle

concentration was maintained at 1% and the hm-chitosan concentration was varied. In this case, the gel modulus G_0 increases linearly with polymer content ($G_0 \sim c_{poly}$), as shown by the plot in Figure 3.5b (the best fit slope is 1.25). The significance of these relationships will be discussed in the next section.

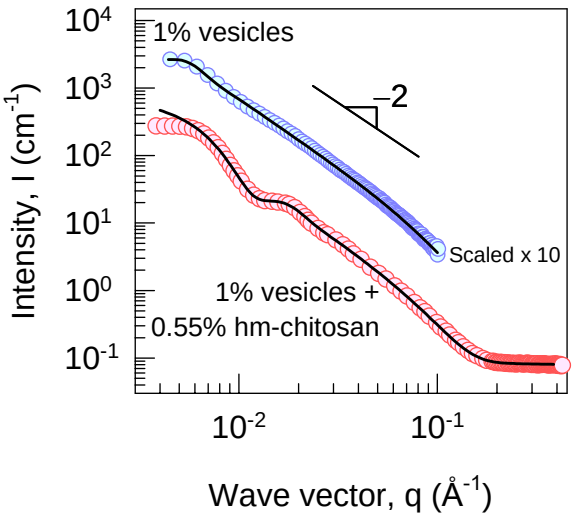

Figure 3.6. SANS data for a vesicle solution and the corresponding gel obtained by adding 0.55% hm-chitosan to this solution. The vesicle solution consists of 1% CTAT/SDBS at a ratio of 70/30. Both samples show the –2 slope characteristic of bilayer scattering.

3.3.2. *SANS*

To probe the microstructure in our samples, we carried out SANS measurements. Samples for SANS were prepared in D_2O to achieve the needed contrast between the microstructure and the solvent. The D_2O samples were visually and rheologically identical to their counterparts made with H_2O. Figure 3.6 shows SANS spectra for the control vesicles (no polymer) and for a vesicle gel made by adding hm-chitosan to those vesicles. In both cases, the scattered intensity $I(q)$ shows

a q^{-2} decay at moderate q, which is characteristic of bilayer scattering (eq 3.3). Data fits using the model for polydisperse unilamellar vesicles (eq 3.4 – 3.6) are shown in Figure 3.6 as solid lines. From the model fit, the vesicles in the control sample (1% CTAT/SDBS at a 70/30 ratio) are seen to have an average radius R_0 of *ca*. 62 nm, with the polydispersity in the radius σ_R, being *ca*. 26%. The bilayer thickness is 2.5 nm and this can be confirmed in a model-independent fashion using a modified Guinier plot of $\ln(Iq^2)$ vs. q^2 as well.[48] The parameters determined here are consistent with previous reports on CTAT/SDBS vesicles.[51]

Turning now to the vesicle gel, we find that its SANS spectrum shows both the q^{-2} dependence at moderate q and the incipience of a form factor minimum at low q. This suggests that the unilamellar vesicles present in the gel are smaller than the control case. From the model fit, we obtain an average vesicle radius R_0 of 18 nm, with the polydispersity in the radius σ_R being about 26%. The bilayer thickness is 2.5 nm as before. Note that we obtain a reasonable fit for the vesicle gel without including a structure factor $S(q)$ in the model, implying that electrostatic or excluded volume effects are not significant for the composition studied. Also, the scattering from vesicles dominates over that from the hm-chitosan in the sample, which is why we can model the data based on vesicles alone. To summarize, the key finding from Figure 3.6 is that the *surfactant vesicles appear to remain intact within the gel*. In addition, the vesicles in the gel appear to be significantly smaller (18 nm radius) than the control vesicles (62 nm radius).

3.4. Discussion

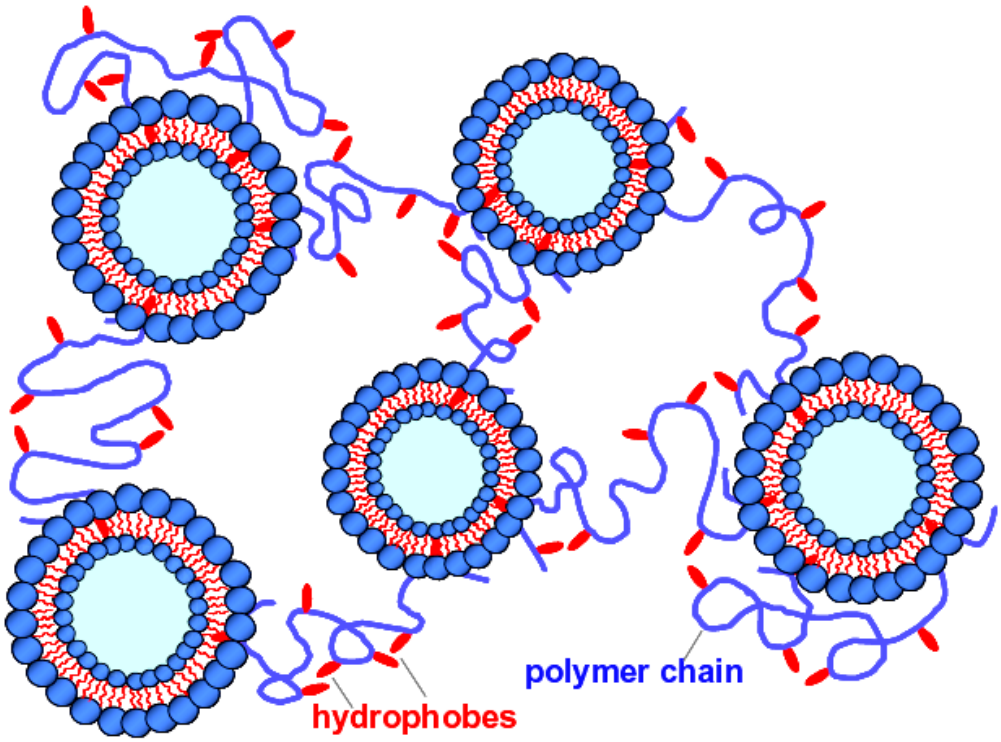

Figure 3.7. Proposed structure of network formed upon addition of hm-chitosan to vesicles. Polymer hydrophobes are shown to be embedded in vesicle bilayers, thus building a connected network of vesicles. Each vesicle acts as a multifunctional crosslink in the network.

The addition of hm-chitosan to surfactant vesicles results in a "permanent" gel, i.e., one that *does not relax* even after infinite time (Figures 3.3d, 3.4). The gel is formed only when the polymer has hydrophobes (Figure 3.4) and we know from SANS that the vesicles remain intact in the gel (Figure 3.6). Based on these findings, the likely structure of the gel is that of a network of vesicles bridged by hm-chitosan chains, as depicted in Figure 3.7. Here, a fraction of the polymer hydrophobes (stickers) are shown to be embedded in vesicle bilayers, so that each polymer chain is connected to two or more vesicles. The vesicles thus serve as multifunctional

crosslinks in a polymer gel network. The permanence of the vesicle gel is probably due to the slow rate of monomer exchange between vesicle bilayers.[18] That is, in contrast to micelles, vesicles do not break and re-form frequently, so that a hydrophobe can remain trapped in a given vesicle for a considerable period of time. Our interpretation of the vesicle gel structure coincides with that of other researchers on similar vesicle-polymer mixtures.[10-14]

To facilitate further analysis, we estimate some relevant length scales in a typical vesicle gel. Consider a 1 wt.% CTAT/SDBS 70/30 mixture with 0.55 wt.% hm-chitosan. Based on the vesicle size (from SANS, Figure 3.6) and concentration, we estimate the distance between adjacent vesicle surfaces to be *ca*. 80 nm. Taking the hm-chitosan next, the contour length of a chain of molecular weight 200,000 is *ca*. 625 nm, assuming a repeat unit size of 0.5 nm.[46] Each chain has about 25 hydrophobes, located about 25 nm apart along the chain. The reported persistence length l_p of hm-chitosan is 7.5 nm at high ionic strength,[46] which implies a radius of gyration R_g in dilute solution of 28 nm. The l_p should be higher in our samples (i.e., the chains should be more rod-like) because our ionic strength is low; thus, our R_g should also be higher. Additionally, for the same molecular weight, the hm-chitosan concentration at overlap c^* is reported to be about 0.1 wt.%.[45,46] Beyond c^*, polymer coils overlap and begin to form "flower micelles". For $c > 10\ c^*$ or so, a viscoelastic network of flower micelles is expected to form, causing a sharp increase in the viscosity.[46] The viscosity of a 0.55 wt.% hm-chitosan solution is relatively low (*ca*.

35 mPa.s, Figure 3.3a) – so at this concentration, the polymer coils are overlapped, but only weakly entangled.

Combining the above calculations, we note that in a typical vesicle gel the distance between two vesicles is much less than the contour length of an hm-chitosan chain and on the same order as its radius of gyration R_g. In such cases, the formation of polymer bridges between vesicles is indeed a plausible outcome. Theories suggest that polymer chains gain conformational entropy when vesicles are at the right distance for bridging, effectively leading to a bridging "attraction".[52-54] In this context, we assume that hydrophobes on the polymer will tend to anchor within the vesicle bilayer, and indeed this is expected to occur provided the hydrophobes are sufficiently long.[42] Moreover, in such cases, the free energy of hydrophobic interactions can overcome electrostatic repulsions between the polymer and the vesicles.[42] This explains why we observe gelation in *like-charged* (cationic) polymer and vesicle mixtures.

Our data for the onset of gelation and for the sol-gel boundary are broadly consistent with the above physical picture. Gelation occurs only above *ca*. 0.05% polymer (the asymptotic y-axis value in Figure 3.2b), which is close to the overlap concentration c^*. Below this concentration, the polymer is able to link a few vesicles, but there are too few chains to form a sample-spanning network. Similarly, gelation occurs only when the vesicle concentration exceeds *ca*. 0.2 wt.% (the asymptotic x-axis value in Figure 3.2b). Below this concentration, the vesicles would be so far

apart that the entropic penalty in stretching polymer chains to bridge vesicles would be excessive. Our sol-gel boundary is comparable to data reported by Porte *et al*.[54] for a similar class of networks, consisting of microemulsion droplets bridged by telechelic associating polymers. The "percolation line" determined by these authors has the same shape and occurs over approximately the same volume fraction range as our sol-gel line.[54] Thus, our sol-gel boundary is suggestive of a percolation threshold, corresponding to the onset of an infinite cluster of bridged vesicles.

We also observe that the vesicle size seems to be modified by the addition of hm-chitosan. Specifically, in the case of the 1% CTAT/SDBS sample (Figure 3.6), the vesicles become much smaller upon adding the hm-chitosan (the radius decreases from 62 nm to 18 nm). This, in turn, implies a sharp increase in the vesicle *number density*, and thereby an increase in the net surface area of the vesicles. The average distance between vesicles is then reduced from *ca*. 150 nm in the control sample to 80 nm in the presence of polymer. We interpret these changes as a response of the system to promote vesicle-polymer interactions. Because the insertion of hydrophobes into vesicle bilayers is energetically favorable, the vesicles rearrange so as to present more surface area to the polymer and thereby accommodate more hydrophobes. At the same time, the reduction in intervesicle distance enables the polymer to bridge adjacent vesicles. The binding of polymer to the outer leaflet of the vesicle may also stiffen the bilayer and thereby stabilize the higher extent of curvature.[55,56] These points are further discussed and reiterated in Chapter 4.

Next, we briefly discuss the observed trends in vesicle gel rheology. The gel modulus G_0 is a measure of the density of elastically-active crosslinks in the gel. We have found that G_0 increases linearly with polymer concentration c_{poly} (Figure 3.5b), a trend observed also by Meier *et al.*[11] for their vesicle gels formed with telechelic polymers. A possible interpretation is that each polymer chain binds to a certain number of vesicles, so G_0 should be proportional to c_{poly} times this number. Note that a very different scaling is expected for an entangled network of polymers or wormlike micelles, where the plateau modulus $G_p \sim c_{poly}^{2.25}$.[38] Thus, the observed linear dependence of the modulus reflects the distinctive nature of the networks studied here, where it is the vesicles that serve as junction points for the polymer chains.

We have also found that the gel modulus G_0 increases with the cube of the vesicle concentration, i.e., $G_0 \sim c_{ves}^3$ (Figure 3.5a). The same cubic relationship has been obtained for the moduli of densely packed unilamellar[57] or multilamellar[58] vesicles. In those cases, the vesicle volume fraction was much higher and the modulus arose from the contact of individual vesicles. Here, it is the polymer chains that build the network, with the vesicles acting merely as junction points in a polymer network. The shear modulus of a semidilute polymer network is $G_0 \approx k_B T/\xi^3$, where $k_B T$ is the thermal energy and the correlation length ξ is associated with the network mesh size.[38] If this relation is assumed to apply for our vesicle gels, it implies that the mesh size varies inversely with the concentration of vesicles, i.e., $\xi \sim 1/c_{ves}$. While this result is interesting, further theoretical work is necessary to explore its meaning and associated ramifications.

Finally, we should add that vesicle gels can be created from all kinds of vesicles. We have prepared lipid vesicles (liposomes) using phosphatidylcholines, and as expected, upon adding hm-chitosan the liposome solution turns into a gel. Controlled release studies from these "liposome gels" will be described in Chapter 5. In other experimental work (data not shown) we have investigated the effect of varying the hm-chitosan molecular weight and the density of grafted hydrophobes. Vesicle gels are formed in all cases, and their gel modulus appears to increase with both polymer molecular weight and hydrophobe density. The vesicle gels are also found to retain their gel-like character over a wide range of temperatures.

3.5. Conclusions

In this Chapter, we have described studies on mixtures of an associating biopolymer, hm-chitosan, with vesicles. The addition of hm-chitosan to vesicle solutions transforms them into elastic gels that can hold their own weight upon tube inversion. These gels retain the bluish color that arises due to light scattering from vesicles, and SANS spectra confirm the existence of vesicles within the gel. The rheological response of the gels is typical of elastic solids, with frequency-independent dynamic shear moduli. The gel modulus increases linearly with polymer concentration and with the cube of the vesicle concentration. It is likely that the microstructure of these gels comprises a network of vesicles connected by hm-chitosan chains, with the hydrophobes on the polymer embedded in vesicle bilayers. Upon adding the polymer, the vesicle appear to re-organize into smaller entities so as to present more surface area for interaction with the polymer hydrophobes.

Chapter 4

Vesicle Morphology Changes Induced by an Associating Biopolymer

A condensed version of this chapter will be published in the following journal article: Jae-Ho Lee, Vivek Agarwal, Arijit Bose, Gregory F. Payne and Srinivasa R. Raghavan, "*Transition from unilamellar to bilamellar vesicles induced by an amphiphilic biopolymer*." Physical Review Letters (**2006**) (in print).

4.1. Introduction

In this chapter, we report further studies with the vesicle gels from Chapter 3. Samples over a range of vesicle and hm-chitosan concentrations are characterized in detail by SANS and by the technique of cryo-TEM. The results from these studies further reinforce the conclusions drawn from Chapter 3, while also indicating additional intricacies. In particular, SANS and cryo-TEM both reveal an interesting transition in the morphology of vesicles from the original *unilamellar* structures to *bilamellar* structures with increasing hm-chitosan to vesicle ratio. The SANS patterns for co-existing vesicles of different lamellarity are particularly unusual, with multiple peaks occurring at high values of the wave vector. We show how to analyze this SANS data by combining existing analytical models for unilamellar vesicles and lamellar phases.

4.1.1. *SANS Modeling of Lamellar Phases* : *Previous Work*

A lamellar phase is a periodic stack of bilayers, as shown in Figure 4.1a. The scattering of radiation from a lamellar phase will be dominated by structure factor effects, which will result in interference peaks in the intensity $I(q)$, as shown schematically in Figure 4.1b. The relative positions of the peaks represent the signature of a lamellar phase – if the first-order peak is located at a wave vector q_0, the second-order peak will be centered around $2q_0$, the third-order peak at $3q_0$ and so on. The wave vector q_0 corresponds to the spacing between the bilayers in the lamellar phase (the d-spacing) via the Bragg relation:

$$d = \frac{2\pi}{q_0} \tag{4.1}$$

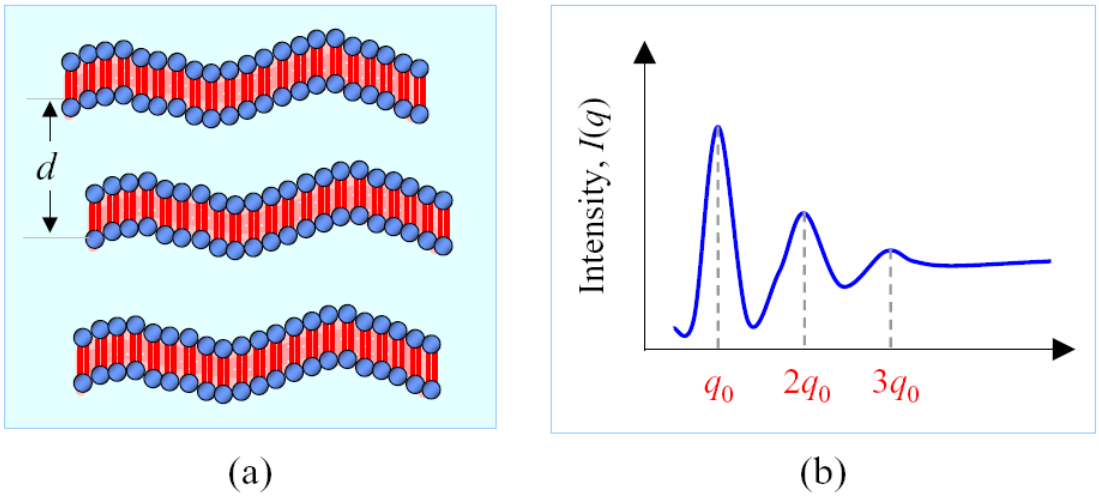

Figure 4.1. (a) Schematic of a lamellar phase, which consists of a periodic stack of bilayers. The bilayers are shown to be fluctuating (undulating) due to thermal motions. The periodicity of the bilayers is represented by the d-spacing, which is indicated in the figure. (b) Typical scattering pattern expected from a lamellar phase. The peak positions occur at integral multiples of the primary peak location q_0. The d-spacing can be obtained from q_0 using Bragg's law.

In addition to the bilayer spacing, it is possible to obtain additional information about the bilayers from their scattering pattern. Consider a periodic stack of N correlated bilayers (i.e., with well-defined bilayer spacing). As the number N increases, the main lamellar peak is expected to grow higher. However, a second factor to be considered is that the bilayers will also be constantly undergoing thermal fluctuations (as depicted in Figure 4.1a). These fluctuations will weaken the inter-bilayer correlations, which will be reflected in the scattering data as a widening of the main lamellar peak and a loss of higher-order peaks. The extent of thermal fluctuations will depend on the rigidity of the bilayers – rigid bilayers will fluctuate weakly, whereas floppy bilayers will show large-amplitude fluctuations. This implies that the scattering data from rigid bilayers should show multiple, sharp peaks, while that from floppy bilayers would show a single diffuse peak.

The above qualitative arguments have been placed on a quantitative footing by Nallet et al.[59] Their model for bilayer scattering provides analytical expressions for the form factor $P_B(q)$ and structure factor $S_B(q)$ of a stack of N bilayers. The total scattered intensity is given by:

$$I(q) = \frac{C}{q^2} \cdot P_B(q) \cdot S_B(q) \tag{4.2}$$

The $1/q^2$ term is the so-called Lorentz factor, and the constant C is related to the area of the basal lamellar plane. The bilayer form factor $P_B(q)$ is given by the equation below, where t is the bilayer thickness and $(\Delta\rho)^2$ is the scattering contrast: [59]

$$P_B(q) = \frac{2\Delta\rho^2}{q^2}\left\{1 - \cos(qt) \cdot \exp\left(-\frac{q^2t^2}{32}\right)\right\} \tag{4.3}$$

The structure factor $S_B(q)$ for bilayers is defined in different ways in the Nallet model depending on whether the number of correlated bilayer stacks N is small or large. For small N, the following expression applies:

$$S(q_z) = 1 + 2\sum_{1}^{N-1}\left\{\left(1 - \frac{n}{N}\right)\cdot\cos(nq_z d)\cdot\exp\left(-\frac{\eta n^2 q_z^2 d^2}{16}\right)\right\} \tag{4.4}$$

where $q_z = q - q_0$. Here d is the d-spacing of the bilayers, which can be independently calculated from the peak positions (eq 4.1). The parameter η is called the Caillé parameter, and is further defined by the equation below:[59]

$$\eta = \frac{q_0^2 k_B T}{8\pi\sqrt{K\cdot\bar{B}}} \tag{4.5}$$

Here k_B is the Boltzmann constant, T the absolute temperature, K the curvature modulus (related to the bilayer bending modulus), and $\bar{B}$ the compression modulus. Thus, the Caillé parameter η is inversely related to a product of two elastic constants characterizing the stiffness or rigidity of the bilayer. The limits for η are from 0 to 1.3, with η = 0 implying very rigid bilayers, and correspondingly, there will be multiple sharp peaks in the scattering pattern. On the other hand, higher values of η correspond to flexible bilayers and in this case, the higher-order peaks may be absent. Note that if the interactions between bilayers are dominated by entropy (i.e., other interactions such as electrostatics are negligible), the bilayers will be quite flexible, and η will follow the simpler geometrical relationship below, which depends only on the d-spacing of the bilayers:[60]

$$\eta = \frac{4}{3}\left[1 - \frac{t}{d}\right]^2 \tag{4.6}$$

4.1.2. *Polymer Effects on Lamellar Phases* : *Previous Work*

A few authors have studied mixtures of associating polymers (polysoaps) and surfactant lamellar phases. Prud'homme et al. found that hydrophobically-modified polyacrylic acid (hm-PAA) was largely miscible with a nonionic lamellar phase, whereas the parent PAA polymer was largely immiscible.[61] The authors studied the hm-PAA samples using SANS and analyzed their data by the Nallet model above. They found that the bilayer rigidity increased systematically with increasing polymer concentration. Ligoure and co-workers have also used the Nallet model to analyze data from mixtures of a lamellar phase and a triblock copolymer.[60]

4.2. Materials and Methods

Sample Preparation. The hm-chitosan polymer and the surfactant vesicles are identical to those used in Chapter 3. The hm-chitosan has a molecular weight around 200,000, and 2.5 mol% of its amines are substituted with n-dodecyl tails. All samples in this study were prepared in D_2O (Cambridge Isotopes). Solutions of the hm-chitosan were made in 1% acetic acid. The vesicles were prepared by mixing solutions of the cationic surfactant, cetyl trimethylammonium tosylate (CTAT) and the anionic surfactant, sodium dodecyl benzene sulfonate (SDBS) in a weight ratio of 70/30 (see Chapter 3 for further details). Vesicle-polymer mixtures of desired composition were obtained by mixing the stock solutions, followed by mild heat.

Small-Angle Neutron Scattering (SANS). SANS measurements were made on the NG-1 (8 m) beamline at NIST in Gaithersburg, MD. Samples were studied at

25°C in 2 mm quartz cells. The scattering spectra were corrected and placed on an absolute scale using calibration standards provided by NIST. The final reduced data is plotted as the radially-averaged, absolute intensity I versus the wave vector q.

Cryo-Transmission Electron Microscopy (Cryo-TEM). Cryo-TEM studies were conducted at the University of Rhode Island using a JEOL 1200EX TEM. Samples were prepared as described in Section 2.4.4. Briefly, a drop of the sample was first placed on a holey carbon film supported on a TEM grid. A filter paper was then used to blot the drop, thus creating a thin film of the sample. The grid was then plunged into liquid ethane to rapidly vitrify the sample. Subsequently, the grid was transferred to a cold stage and maintained at –170°C in the TEM for observation.

4.3. Results and Discussion

4.3.1. *SANS Data and Modeling*

We present SANS data for vesicle + hm-chitosan mixtures as a function of polymer concentration (Figure 4.2) and vesicle concentration (Figure 4.3). The data is presented for the absolute intensity I as a function of the scattering vector q. In Figure 4.2, the vesicle concentration is held constant at 0.5%. Data are shown for the control sample (vesicles, no polymer) and for four different polymer concentrations. The curves are scaled by factors of 10 for easy identification. In Figure 4.3, the polymer concentration is held constant at 0.55%, while the vesicle concentration is varied from 1.4% to 0.2%. The data in Figure 4.3 is shown unscaled – the curves are well-separated because the number of scatterers (vesicles) per unit volume is increasing.

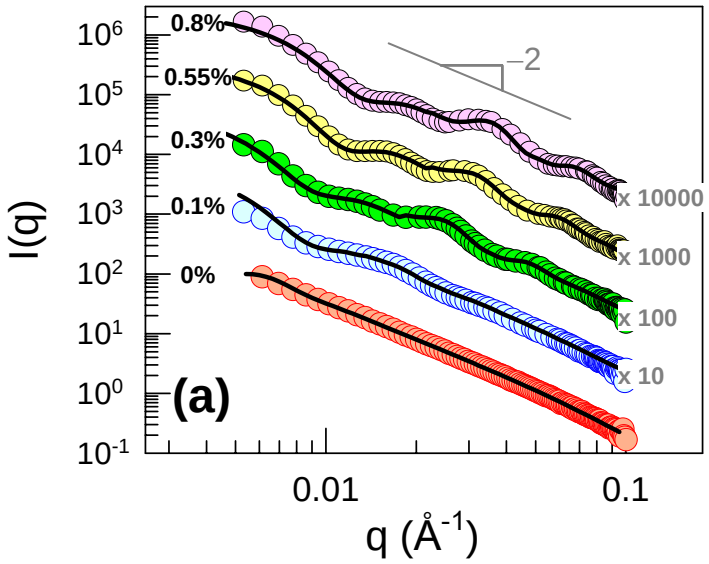

Figure 4.2. SANS data from vesicle-polymer mixtures as a function of the polymer (hm-chitosan) concentration. The vesicle concentration is held constant at 0.5%. Data is shown for the following polymer concentrations and data is shown for the polymer concentration indicated. Successive curves are offset by factors of 10 for clarity. Lines are fits to appropriate models.

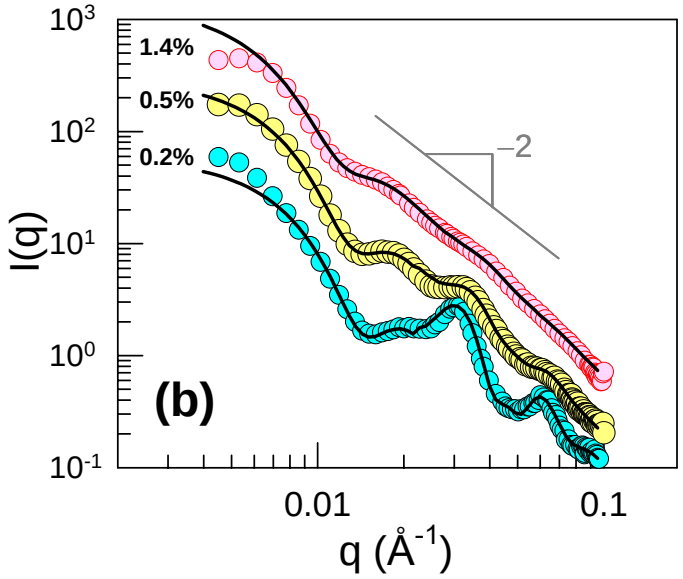

Figure 4.3. SANS data from vesicle-polymer mixtures as a function of the vesicle concentration. The polymer (hm-chitosan) concentration is held constant at 0.55%. Data is shown for the vesicle concentrations indicated. Lines are fits to appropriate models.

We now discuss the interpretation and modeling of these spectra. Consider first the control vesicles (Figure 4.2). In the dilute, non-interacting limit, the structure factor $S(q) \rightarrow 1$ and we can model the data based on the form factor for unilamellar vesicles (ULVs) of radius R and bilayer thickness t, as described in Section 3.2.1. For thin bilayers, $P(q)$ is given by eq 3.3, according to which $I(q)$ should show a q^{-2} decay in the low q range. To account for polydispersity in the vesicle size, $P(q)$ can be averaged over a Schultz distribution (eq 3.4–3.6), where the spread in vesicle sizes is measured in terms of a polydispersity index p. In Figure 4.2, the fit from the polydisperse ULV model is shown for the 0.5% vesicle solution. Note that the data follows a slope of –2 at low q. From the model, the average vesicle diameter $\bar{D}$ is found to be 117 nm and the bilayer thickness t is 2.5 nm (see Table 4.1).

Table 4.1. Parameters from SANS Modeling of Vesicle-Polymer Mixtures

Concentrations		**Type of fit**	**ULVs**			**MLVs**		
Vesicles	Polymer		Avg. dia.	Bilayr. thick.	Polydisp.	d-spacing	Stack no.	Caille param.
c_v (%)	c_p (%)		D (nm)	t (nm)	p	d (nm)	N	η
0.5	0	ULV	117	2.5	0.25	-	-	-
0.5	0.1	ULV	53	2.5	0.30	-	-	-
0.5	0.3	ULV + MLV	52	2.5	0.30	25.0	2.5	0.50
0.5	0.55	ULV + MLV	40	2.5	0.24	18.4	2.6	0.45
0.5	0.8	ULV + MLV	39	2.5	0.27	17.5	3.0	0.40
0.2	0.55	ULV + MLV	39	2.5	0.21	19.9	3.0	0.29
0.5	0.55	ULV + MLV	45	2.5	0.25	19.9	2.4	0.40
1.4	0.55	ULV	39	2.5	0.30	-	-	-

Next, we apply the polydisperse ULV model to vesicle-polymer mixtures in cases where the polymer:vesicle ratio is low. For the samples with 0.5% vesicles +

0.1% polymer (Figure 4.2) and 1.4% vesicles + 0.55% polymer (Figure 4.3), the model yields a very good fit. From the data, we note that the addition of polymer reduces the vesicle size significantly (see Table 4.1). For example, adding 0.1% polymer to a 0.5% vesicle solution reduces the mean vesicle diameter $\bar{D}$ from 117 nm to 53 nm. Such a reduction in ULV size upon addition of polymer was inferred in Chapter 3 as well, and possible reasons were discussed earlier in Section 3.4.

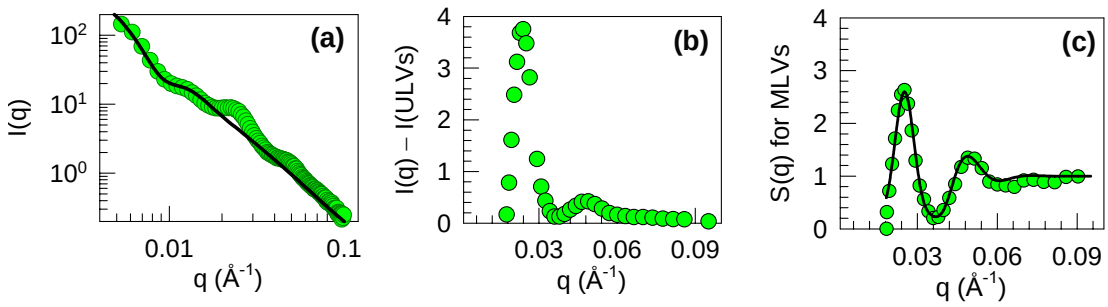

Figure 4.4. Typical modeling procedure for data corresponding to a mixture of unilamellar (ULVs) and multilamellar vesicles (MLVs). The sample is a mixture of 0.5% vesicles and 0.55% hm-chitosan. (a) The low q data is fit to a ULV model; (b) The difference between the overall data and the ULV model is shown; (c) The structure factor contribution to the curve in (b) is shown, and the line through this data is a fit to the Nallet model (eq 4.4).

A further striking feature appears in the SANS data at higher polymer:vesicle ratios – *viz*., the emergence of two peaks at higher values of q, with the peak positions showing a "lamellar" spacing (first peak at q_0, second at $2q_0$). We will show that the appearance of these high q peaks implies the formation of multilamellar vesicles (MLVs) with well-defined bilayer spacing. To model a mixed population of unilamellar vesicles (ULVs) and MLVs, we adopt the following procedure, illustrated in Figure 4.4. Two assumptions are inherent to our analysis: (a) the scattering from

the two types of vesicles is additive; and (b) the MLVs contribute to the scattering only on account of their bilayers. In other words, the MLVs are assumed to be so large that their overall size falls outside the range probed by SANS, which would allow us to neglect their contribution to the scattering at low q.

The data shown in Figure 4.4a is for the sample with 0.5% vesicles + 0.3% polymer (from Figure 4.2). First, we apply the ULV model to the low-q data, ignoring the high-q peaks. Note that the fit is excellent at low-q, and the fit gives an average vesicle diameter of 52 nm (Table 4.1). Next, we subtract the ULV fit from the total intensity, and the resulting data is shown in Figure 4.4b. This data corresponds to the MLVs, and it closely resembles the scattering from a lamellar phase, with peaks at q_0 and $2q_0$. To model this data, we use the Nallet model, described earlier in this Chapter. The first step in this process is to calculate the bilayer form factor $P_B(q)$, which is given by eq 4.3 (the bilayer thickness t is assumed to be that of the ULVs). Then, we substitute the measured intensity $I(q)$ and the calculated $P_B(q)$ into eq 4.2 to obtain the structure factor $S_B(q)$ for bilayers, which is normalized such that it asymptotically approaches 1. This data, shown in Figure 4.4c is then fit to the Nallet expression for $S_B(q)$ (eq 4.4), which is valid for a small number of bilayer stacks N. Note that the two parameters in this model are N and the Caillé parameter η (which is inversely related to the bilayer rigidity). The parameter d in eq 4.4 is the d-spacing of the bilayers, which is obtained directly from the peak position through the Bragg relation (eq 4.1).

The above analysis was applied to all samples that showed high-q peaks, and corresponding values of N, η and d for these samples are given in Table 4.1. Also, combined fits incorporating both the ULV and MLV models are shown as solid lines through the $I(q)$ data for each sample in Figures 4.2 and 4.3. Turning to Table 4.1, the first point to be noted is that the values of the stack number N range from 2.4 to 3. Note that the fractions represent linear combinations of the Nallet model for the integral values of N = 2 and 3. This implies that there are between two and three bilayers in each of our MLVs. The fact that peaks appear in SANS despite the small number of bilayers suggests that the bilayer spacing is tightly controlled. Further analysis of trends in d and h are discussed later. But first, we present data from cryo-TEM that corroborate the above SANS result of a small, finite number of bilayers per MLV.

4.3.2. *Cryo-TEM Data*

Typical images of our samples are shown in Figure 4.5. As expected, the control CTAT/SDBS sample shows polydisperse unilamellar vesicles, with diameters ranging from 60–100 nm. However, in the 0.5% vesicles + 0.3% hm-chitosan sample, two types of vesicles are seen. On the one hand, there are a number of unilamellar vesicles (ULVs) with diameters ranging from 20–60 nm. In addition, there are also larger *bilamellar* vesicles (BLVs), i.e., vesicles with two concentric bilayers, with diameters exceeding 100 nm. A similar mixture of ULVs and BLVs are seen in the three images of the 0.5% vesicles + 0.55% hm-chitosan sample. Again, the ULVs are quite small (20–50 nm diameter) compared to the BLVs. A number of the BLVs are

seen to be elongated structures – this may be a result of the shear caused by the blotting during sample preparation.[62] We should emphasize that mixtures of ULVs and BLVs were seen in virtually all images collected for this sample.

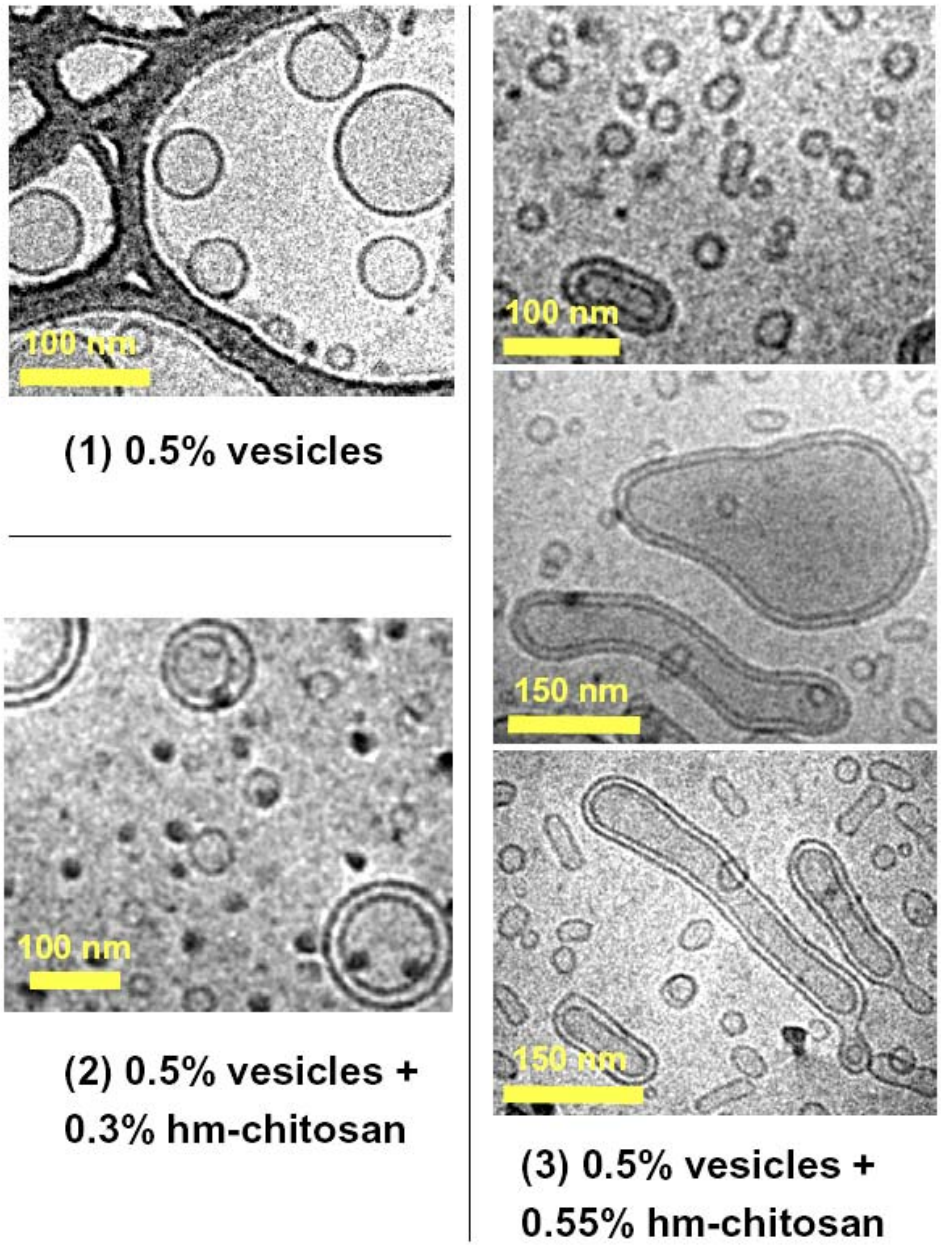

Figure 4.5. Cryo-TEM images of the control vesicles (**1**) and vesicle-polymer mixtures (**2**, **3**). Samples **2** and **3** show a co-existence of unilamellar vesicles (which are smaller than the control case) and bilamellar vesicles.

It is significant that the cryo-TEM images reinforce the conclusions obtained from SANS modeling. Specifically, the images confirm that (i) adding polymer reduces the sizes of the ULVs relative to the control vesicles; and (ii) at higher amounts, the polymer also induces the formation of bilamellar vesicles (BLVs) that co-exist with the ULVs (in rare instances, trilamellar vesicles were also seen). It also appears that the spacing between bilayers is identical in all the BLVs, confirming our hypothesis that this spacing must be tightly controlled to result in SANS peaks. Because of the shear associated with cryo-TEM sample preparation, a more quantitative comparison between the SANS and cryo-TEM data is not possible. Nevertheless, the qualitative agreement is encouraging.

4.3.3. *Analysis of Parameters from SANS Modeling*

Further insight into our system can be obtained by discerning trends in the parameters obtained from SANS modeling. First, at a constant vesicle concentration of 0.5%, the *d*-spacing between the bilayers in the MLVs steadily decreases with increasing polymer concentration (Table 4.1). This point is underscored by the data in Figure 4.6a, where the bilayer structure factor $S_B(q)$ is plotted for three different polymer concentrations with the vesicle content being fixed at 0.5%. We note that the position of the primary lamellar peak (q_0) moves to higher values of the wave vector as the polymer concentration is increased, indicating a decrease in the *d*-spacing. The plot in Figure 4.6b shows that the *d*-spacing decreases with polymer concentration according to a power law with a slope of approximately –1/3. The same trend in *d*-spacing has been observed in other related studies with lamellar phases.[63]

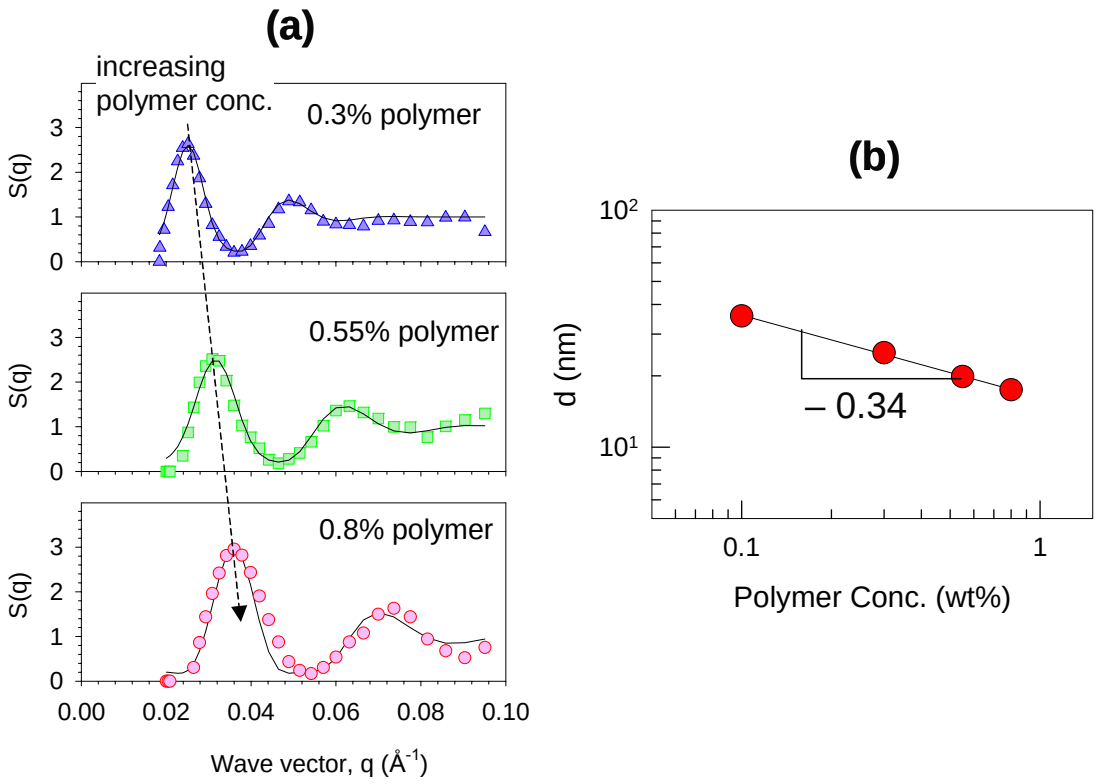

Figure 4.6. (a) Structure factors for three vesicle-polymer mixtures at a constant vesicle concentration of 0.5% and varying hm-chitosan concentrations. Note that the position of the primary peak moves to increasing wave vectors with increasing polymer concentration, indicating a decrease in the *d*-spacing of the bilayers. (b) Plot of the above *d*-spacings vs. polymer concentration. The *d*-spacing decreases according to a power law with a slope of about –1/3.

Next, we consider trends in the Caillé parameter η, which is observed to decrease systematically from around 0.8 to a plateau around 0.4 with increasing polymer:vesicle ratio (this is reflected as a slight sharpening of the SANS peaks). As shown by eq 4.5, η is an inverse measure of bilayer rigidity, and a decrease in η implies that the bilayers become more rigid. A similar increase in bilayer rigidity upon addition of associating polymer was found by Prud'homme et al.[64] (see Section 4.1.2). Table 4.1 also indicates a weak trend in the number of bilayer stacks *N*, which shows a small but systematic increase with increasing polymer:vesicle ratio, inching

closer to 3 at high ratios. Lastly, with regard to the size of the ULVs present, the average ULV diameter decreases to *ca*. 40 nm upon adding just a small amount of polymer and remains around this value with further polymer addition.

4.3.4. *Mechanism for Structural Transitions*

Based on the above trends, we can put forward a tentative mechanism to explain the structural changes observed in our system. At low amounts of hm-chitosan, the vesicles tend to be decorated with a few hm-chitosan chains that have inserted some of their hydrophobes into the vesicle bilayers. These chains extend between adjacent vesicles and thereby connect and network these vesicles. On account of the embedded polymer chains, the bilayer becomes more rigid, which explains the decrease in η.[61] In turn, the increase in bilayer rigidity serves to stabilize a higher curvature (smaller average size) for the vesicles, as has been observed by others.[55] This can explain why the average vesicle size decreases. The same arguments were made earlier in Chapter 3.

As more polymer is added, we suggest that a different scenario could occur. At this point, numerous polymer chains are likely to be bound to each vesicle, and there are possibly multiple connections between any two adjacent vesicles. The vesicle size cannot drop indefinitely (a limiting curvature is apparently reached when the diameter falls to ca. 40 nm). We suggest that instead, the polymer chains connecting adjacent ULVs induce their fusion into bilamellar structures (BLVs) having inner and outer membranes. The sequence of events with increasing polymer

concentration are depicted in Figure 4.7. Note that only a fraction of the ULVs fuse into BLVs, and the two types of structures co-exist. Each BLV is evidently formed from several smaller ULVs, with the polymer chains bridging the two bilayers.

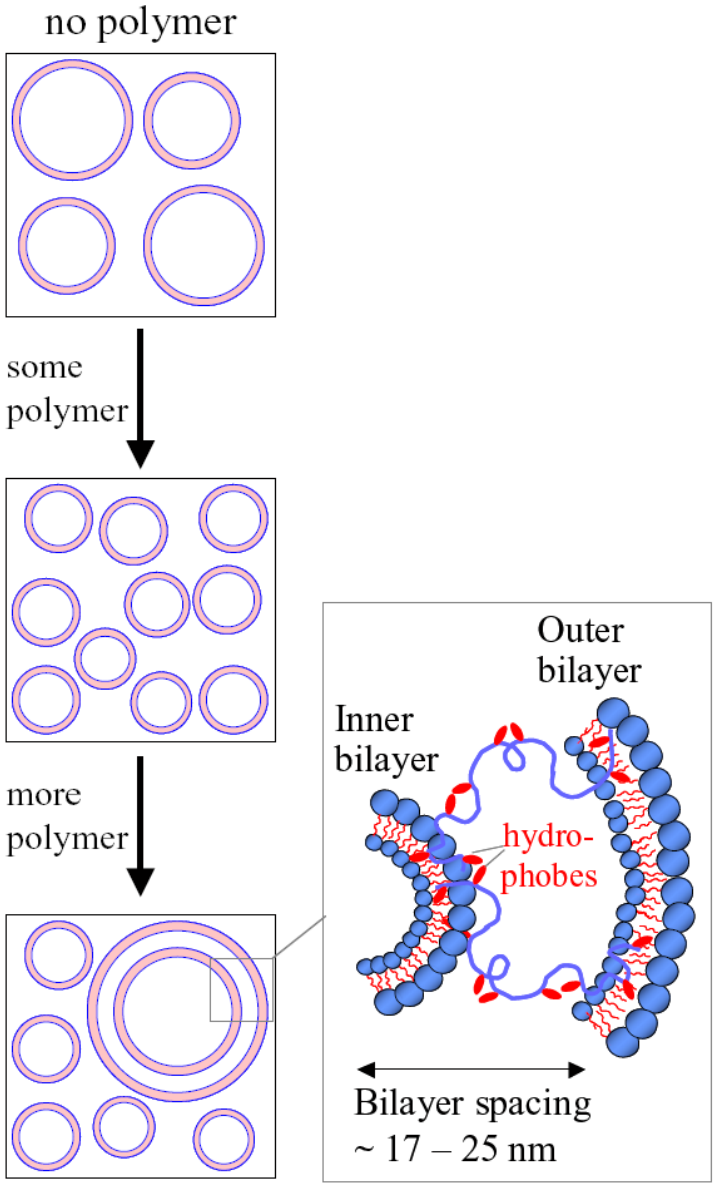

Figure 4.7. Schematic of the transitions occurring in vesicle morphology upon addition of associating polymer. First, the size of ULVs decreases. At higher polymer content, a few BLVs are formed that co-exist with the ULVs. For clarity, the polymer chains connecting the vesicles are omitted on the left, but are shown on the right.

It is worth emphasizing that at the onset of BLV formation, the *d*-spacing between the bilayers in the BLVs is comparable to the polymer's radius of gyration (ca. 30 nm, see Chapter 3). With further polymer addition, the bilayer spacing systematically decreases – presumably, this is because bilayers that are covered by polymer chains to a greater extent experience an attractive "pull" towards each other. In other words, by bringing the bilayers closer, the polymer chains get to maximize the favorable contact between their hydrophobes and the confining bilayers, even if the chains must sacrifice some configurational entropy as they get squeezed a bit in the process.

It is interesting to speculate on a possible connection with biological systems. Membranes that enclose cellular organelles are known to contain both lipids and amphiphilic macromolecules, such as membrane proteins.[25] Interestingly, several organelles in eukaryotic cells are bilamellar, i.e., have a double membrane structure. These include the nucleus, the mitochondria, and the chloroplasts in plant cells. At the same time, these bilamellar organelles co-exist in a cell with numerous unilamellar (single membrane) organelles, such as lysosomes, endosomes, and Golgi bodies.[25] Why are only certain organelles bilamellar, and in those organelles, how is the spacing between the inner and outer membranes regulated? Although these issues are not fully understood at the moment, we can speculate that a key role might be played by amphiphilic macromolecules (e.g., membrane-bound proteins) in a similar way as reported in this study.

4.3.5. *Stability of Vesicle Co-Existence: Aging Effects*

One last issue that we will touch on here is the issue of sample stability. The mechanism proposed above for the structural changes ascribed them to essentially thermodynamic forces (changes in bilayer rigidity, curvature, etc.). But can ULVs and BLVs indeed show a stable co-existence? Given time, will the ULVs aggregate and turn into BLVs, or into vesicles of an even higher lamellarity?

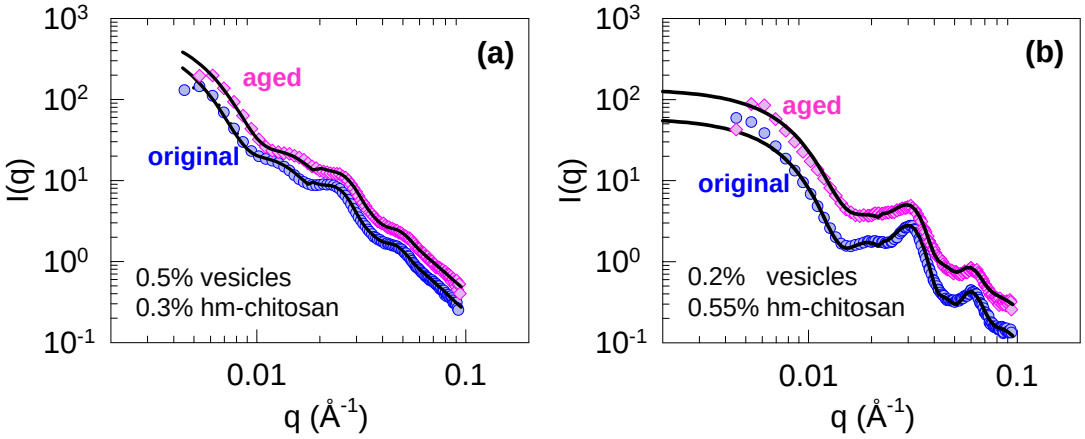

Figure 4.8. SANS data for two vesicle-polymer samples taken more than one year after they were originally prepared. The original data is shown for comparison.

To examine these issues, we have conducted SANS studies on vesicle-polymer samples that were aged for more than one year (samples were stored at room temperature in the intervening period of time). Data for two such samples are shown in Figure 4.8, comparing the original and the aged responses (the data is shown unscaled). We note that the responses are approximately identical, with the aged sample having a slightly higher intensity. Modeling of the above data show that the ULVs in the aged sample are slightly smaller (average radius ca. 5 nm lower). With

regard to the MLVs, the *d*-spacing, stack number, and the Caillé parameter are approximately the same for both cases. Also, both the original and aged samples were visually seen to be clear, viscous fluids – i.e., there was no macroscopic phase separation over a one year period. The results suggest that a stable co-existence of vesicles of different lamellarity is indeed possible over significant periods of time, much like is observed for cellular organelles.

4.4. Conclusions

We have shown in this Chapter that the addition of an associating biopolymer can cause changes in the size and morphology of unilamellar vesicles (ULVs). The polymer binds to vesicles, causing the bilayer to rigidify and in turn driving a decrease in the size of ULVs. At higher polymer:vesicle ratios, the polymer induces the fusion of some ULVs to form bilamellar vesicles (BLVs). The co-existence of ULVs and BLVs in the sample leads to a striking pattern in SANS with multiple peaks, and modeling of this SANS data corroborates such a vesicular co-existence. Moreover, these structures have been directly visualized by cryo-TEM. Samples with co-existing ULVs and BLVs appear to be quite stable over more than a year. A possible connection is noted with the stable co-existence of uni- and bilamellar organelles within eukaryotic cells.

Chapter 5

Vesicle-Biopolymer Capsules and Gels: Controlled Release Studies

5.1. Introduction

In Chapters 3 and 4, we have studied the microstructure and rheological properties of vesicle gels. As mentioned in Chapter 1, one of our motivations for studying these materials is due to their potential utility in drug delivery and other controlled release applications. Towards this end, we investigate in this Chapter the release kinetics of model hydrophilic dyes encapsulated in vesicle gels. In addition, we turn our attention to a second type of structure, viz. biopolymer capsules loaded with vesicles. Capsules are obtained by combining chitosan with an anionic biopolymer, and the loading of vesicles into these capsules results in a hybrid container-within-container structure. Again, we study the release kinetics of model dyes from these hybrid capsules. Also, to facilitate the use of capsules in targeted drug delivery, we make magnetic capsules containing magnetic nanoparticles. Additionally, we demonstrate a method to covalently attach antibodies to the capsule surface for biomolecular targeting to specific tissues. Altogether, the studies in this Chapter suggest that both vesicle gels and vesicle-loaded capsules could be useful in drug delivery and controlled release applications.

5.1.1. *Drug Delivery From Vesicle Gels: Previous Work*

Vesicles are known for their ability to encapsulate desired chemicals, both hydrophilic moieties within their aqueous core, as well as hydrophobic moieties within their bilayer shell. These chemicals will tend to slowly leak out through the bilayer into the external fluid, thereby providing a convenient mechanism for sustained release. For drug delivery applications, vesicles are usually made from lipids (the term "liposome" is commonly used for lipid vesicles), since lipids tend to be naturally occurring and biocompatible components. One problem with vesicle-based drug delivery has been the rapid clearance of vesicles from the bloodstream by the reticuloendothelial system (RES).[65] A partial solution to this problem is to coat the vesicles with polyethylene glycol (PEG), which is found to significantly enhance the circulation time of vesicles in blood (the exact mechanism for this is not well understood).[8,65-68] Nevertheless, the limited stability of vesicles to external conditions such as pH, temperature or ionic strength still can cause the drug in the vesicles to be released too rapidly or at undesired sites within the bloodstream. There is hence a need to find mechanisms to stabilize vesicles.

One possible mechanism to impart greater stability to vesicles is to *embed them in a polymer gel matrix*. In this case, there are no active connections between the polymer gel strands and the vesicles, unlike our vesicle gels in Chapters 3-4, where the vesicles play an active role as crosslinks in the gel network. The latter type of "active vesicle gel" has not been investigated for drug delivery to our knowledge. However, the former, i.e., "vesicles embedded in gels", has been studied by a number

of researchers. The first report of vesicles in a gel was by Weiner *et al*. who embedded lipid vesicles containing hormones in a collagen matrix.[69] They found that their hybrid gel prolonged the retention time of hormones. Following this study, vesicles have been encapsulated in gels of various kinds, including gels of biopolymers such as xanthan gum, chitosan, and carboxy-methylcellulose, as well as gels of synthetic polymers such as Carbopol.[69-71]

Only a few commercial applications have been reported so far for gels containing embedded vesicles. The majority of these involve topical applications, with the vesicles serving to facilitate drug absorption into skin. Another application was recently described by Di Tizio et al., where vascular and urinary catheters were coated with a gel with embedded drug-containing vesicles. The authors showed that such a coating could minimize the risk of infection.[72]

It is worthwhile to evaluate the factors necessary for the "vesicles in a gel" concept to be used in drug delivery. First, the vesicles should remain stable in the gel under physiological conditions (temperature of 37.6°C, pH of 7.4, ionic strength of 0.25 M). Second, the polymer forming the gel should itself be biocompatible and biodegradable. Third, the gel stiffness and strength should be sufficiently high for the application of interest. If these conditions are met, the vesicles could indeed be "protected" by the gel matrix, and the release of encapsulated drug from within the vesicles could be prolonged due to the combination of transport resistances across the vesicle bilayer and through the gel matrix. As noted above, the vesicle gels described

in Chapter 3-4, where vesicles are connected by associating biopolymer (hm-chitosan) chains, have not been evaluated for drug delivery applications to our knowledge. Chitosan, as detailed earlier, is considered to be a biocompatible and biodegradable polymer. We will therefore evaluate vesicle gels formed using lipid vesicles and hm-chitosan as a controlled release matrix.

5.1.2 *Drug Delivery from Vesicle-Loaded Capsules*: *Previous Work*

Polymer capsules ranging in size from a few microns to several millimeters can be prepared by several methods such as solvent evaporation, coacervation, ionic gelation and spray drying.[73,74] Capsules have been made from biopolymers such as chitosan, gelatin, agarose, and alginate, and synthetic polymers such as polylactic acid (PLA), polylactic–co-glycolic acid (PLGA), and polyvinyl alcohol (PVA). Structurally, capsules have a thin shell enclosing a water-filled interior. Drugs or macromolecules (proteins, hormones) can be encapsulated in the interior and delivered at a controlled rate.

Capsules made from the polysaccharide, alginate have proven to be particularly popular, both for drug delivery applications as well as to immobilize cells for tissue engineering applications. These capsules are formed by **ionic crosslinking**, whereby a solution of sodium alginate is dropped into a solution of a divalent cation, typically calcium (Ca^{2+}). In the process, the interface of the added drop is crosslinked by the calcium ions, resulting in an interfacial shell. The drug-release rate from alginate capsules can be controlled by varying the concentrations of the alginate and

the calcium ions. *In vivo* studies with alginate capsules have shown that they are biocompatible, non-toxic, and biodegradable over the long term.[75]

Capsules can also be formed by **polyelectrolyte complexation** – a process that requires two biopolymers of opposite charge, or one biopolymer and a surfactant of opposite charge (the overall process is similar to that for alginate/Ca^{2+} above). For example, one could use sodium alginate, which is an anionic polymer, and either chitosan or poly-L-lysine (PLL), which are cationic polymers. To form the capsules, a solution of sodium alginate is added dropwise to a solution of chitosan. The contact between the oppositely charged polymers at the drop interface induces an electrostatic crosslinking, which gives rise to a polymer shell around the drop. In this way, capsules of given size (equal to the size of the generating drop) can be created readily by a simple, mild process (at room temperature, without using organic solvents), and it is straightforward to encapsulate drugs in the capsule in this method.

Our interest lies in capsules with *encapsulated vesicles*. Note that capsules can protect vesicles from external stimuli, such as low or high pH, and from destruction by agents such as macrophages. Also, vesicles may extend the functionality of capsules, since they are more effective at encapsulating hydrophobic drugs (such as many anti-cancer formulations) than the capsules themselves. Finally, the combination of transport resistances from the vesicle bilayer and the capsule shell can again prolong the release of encapsulated drug.

The Langer group were the first to show that vesicles could be trapped in alginate microcapsules and that dye encapsulated in the vesicles could be released slowly under certain conditions.[76,77] Subsequent studies from the same group showed that micro-encapsulated vesicles could extend the *in vivo* drug release time and minimize immune responses.[78] The concept of "vesicles in capsules" has been used thereafter by other researchers.[17,79,80] Cohen et al.[79] encapsulated vesicles into alginate-PLL capsules. They found a higher release rate from anionic vesicles compared to cationic vesicles. The slower release rate in the latter case was attributed to binding of cationic vesicles with the anionic alginate chains in the capsule matrix.

More recently, Dhoot et al.[81] have studied the effect of crosslinking ions on release rates of fluorescein-isothiocyanate labeled bovine serum albumin (FITC-BSA) from vesicle-loaded alginate capsules. A rapid initial burst of the FITC-BSA protein was observed when alginate capsules were made with Ca^{2+}, Al^{3+}, and Ba^{2+}. The release rate of the protein was found to differ based on the type of ions used in generating the capsules.

Lastly, we wish to point out the recent report by Ramadas et al.[82] who have used vesicle-loaded alginate-chitosan capsules for oral delivery of insulin. These capsules were able to deliver insulin to the intestine without undergoing degradation in the acidic environment of the stomach. This provides an example where the capsules serve as a protective barrier for the vesicles and their encapsulated contents.

5.2. Materials and Methods

Polymers. The chitosan and the hm-chitosan were identical to those used in Chapters 3 and 4 (from Sigma, molecular weight 200,000, degree of deacetylation 80%). The graft density of n-dodecyl hydrophobes on the hm-chitosan was 2.5 mol%. Glycerol phosphate (GP) and glutaraldehyde (GA) (both from Aldrich) were used as physical crosslinking agents for the chitosan. The gelatin used to prepare capsules was purchased from Sigma and was of grade 300 bloom.

Surfactant Vesicles. The surfactant vesicles were also the same as those studied in earlier chapters, and were prepared by mixing the cationic surfactant, cetyl trimethylammonium tosylate (CTAT) and the anionic surfactant, sodium dodecyl benzene sulfonate (SDBS) in a weight ratio of 70/30.

Lipid Vesicles. The lipid, egg-yolk phosphatidyl choline (EPC) was purchased from Avanti Polar Lipids. Large unilamellar vesicles (LUVs) of the lipid were prepared according to the reverse-phase evaporation method.[83] First, a lipid film was deposited on a vial by evaporation under a nitrogen atmosphere. The film was then redissolved in diethyl ether and an aqueous solution of 20 mM HEPES buffer (HEPES = 4-(2-hydroxyethyl)-1-piperazineethane-sulfonic acid; from Sigma) was added. The mixture was sonicated to get a homogeneous solution, and the diethyl ether was then removed under vacuum. This solution contains a polydisperse mixture of vesicles. To obtain vesicles of a given size, the above solution was extruded through a membrane filter of given pore size (typically 100 nm), which finally gives us lipid vesicles with a size identical to the pore size of the filter.

Encapsulating Dye in the Vesicles. The two fluorescent dyes, calcein and 6-carboxy-fluorescein (CF) were obtained from Sigma. The chosen dye was added to the aqueous solution used in preparing either lipid or surfactant vesicles. A dye concentration of 100 mM was used with lipid vesicles and 0.5 mM with surfactant vesicles. In the process of forming vesicles, some of the dye remains encapsulated in the vesicles, while the majority of the dye diffuses freely outside the vesicles. The latter free dye was removed by size exclusion chromatography (SEC) using a Sephadex G-50 column (medium mesh, Amersham Bioscience).

Preparation of Vesicle Gels. Vesicles with encapsulated dye were combined with hm-chitosan solution, and the mixture was mildly heated at 50°C for two hours, followed by centrifugation to remove bubbles.

Preparation of Capsules and Vesicle-Loaded Capsules. The preparation of biopolymer capsules with hm-chitosan as the cationic biopolymer and gelatin as the anionic biopolymer is discussed in the Results section (5.3.3). The loading of vesicles into these capsules is also described in this section.

Preparation of Magnetic Capsules. The γ-Fe_2O_3 particles used in preparing magnetic capsules were purchased from Alfa Aesar. Their size was specified to be 32 ± 18 nm, and their average surface area was 42 m^2 /g. The particles were dispersed at a concentration of ca. 0.1 to 0.2 wt% into the capsule forming solution using a high-shear mixer (Tissue Tearor) for about 30 s. The dispersion was then centrifuged

to remove bubbles and then used immediately for preparing capsules. Further details on magnetic capsule preparation are described in Section 5.3.4.

Preparation of Antibody-Functionalized Capsules. Fluorescein-labeled goat anti-mouse immunoglobulin (FL-anti-mouse-IgG), mouse IgG, and Alexa Fluor 568 succinimidyl ester (AF) were purchased from Invitrogen. AF labeled-mouse IgG was synthesized using methods described by the dye supplier.[84] Briefly, mouse IgG (2.5 mg/ml) was purified and brought to pH 8.5 using sodium bicarbonate buffer. Then, 1 mg of AF dissolved in 0.1 mL of dimethylsulfoxide (DMSO) was added and mixed for 1 h. The resulting AF-mouse-IgG was purified using a Sephadex G-25 chromatography column to remove unreacted AF. AF-mouse-IgG was attached to capsules using glutaraldehyde (GA) as a bifunctional linker (details in Section 5.3.5). To image the antibody-coated capsules, fluorescence microscopy was used on a Leica MSFLIII microscope. For the FL dye, the excitation wavelength was fixed at 480 nm with a 40 nm bandwidth, and an emission cutoff filter at 510 nm was used. For the AF dye, the excitation wavelength was 560 nm with a 40 nm bandwidth, and an emission cutoff filter at 610 nm was used.

Dye Release Studies. Dye release studies from vesicle gels and capsules are described in detail in the Results section. Phosphate-buffered saline (PBS) solution from Aldrich was used as the continuous medium. UV-Vis spectroscopy on a Varian Cary 50 spectrophotometer was used to monitor the dye concentration, with samples placed in 1 cm cuvettes. To disrupt vesicles (e.g., for determining the total dye concentration), the detergent, Triton X-100 (from Aldrich) was used.

5.3. Results

5.3.1. *Vesicle Gel Formation Using Lipid Vesicles*

Our initial studies in Chapter 3 used CTAT/SDBS surfactant vesicles, which are easy to prepare and work with as they are formed spontaneously and are indefinitely stable. For drug delivery applications, however, it is important to use vesicles made from natural lipids. But regardless of the type of vesicles (surfactant or lipid), we do observe gel formation upon adding hm-chitosan to the vesicles. For example, when EPC lipid vesicles at a concentration of 0.5% are mixed with a 0.7% hm-chitosan solution, we obtain a bluish gel that supports its own weight in an inverted vial. Dynamic rheological data (not shown) confirm that this sample is a gel with a plateau in the elastic modulus G' at low frequencies. The modulus of lipid vesicle gels increases linearly with vesicle concentration, in much the same way as was found for surfactant vesicles (Figure 3.5, Chapter 3). Thus, vesicle gels seem to behave in a similar manner, whether they are formed from lipid or surfactant vesicles.

5.3.2. *Dye Release from Vesicle Gels*

We now describe dye release studies from vesicle gels. A CTAT/SDBS vesicle gel containing the dye, calcein inside the vesicles (no free dye) was placed in the bottom of a 3.5 mL vial, and the headspace above the gel was filled with 2.5 mL of a phosphate buffered saline (PBS) solution at pH 7.1 (Figure 5.1a). The PBS was used to simulate a physiological environment that would be encountered, for instance, by a gel implanted in the body. The entire vial was placed in a water bath at 37°C. As

time progresses, the dye from the gel diffuses into the supernatant, and the concentration of dye in this supernatant was continuously monitored by UV-Vis spectroscopy.

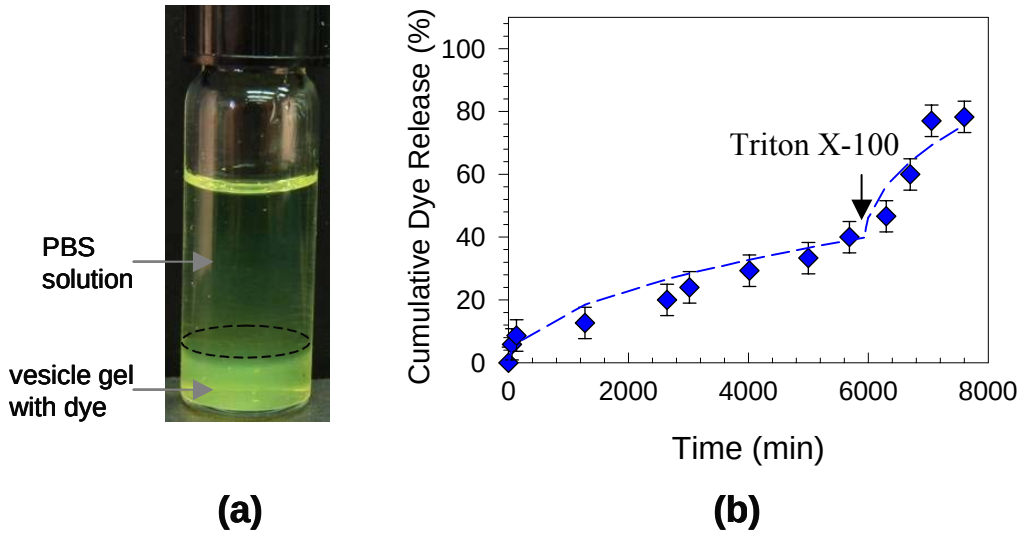

Figure 5.1 (a) Photograph showing the boundary between a PBS solution (supernatant) and a vesicle gel. (b) Calcein release profile from a surfactant vesicle gel. The lines are to guide the eye.

We should point out that in Figure 5.1a, there is a clear interface between the vesicle gel and the PBS solution. This means that the vesicle gel is stable when placed in contact with the PBS solution, and does not "dissolve" away with time (thereby ensuring that we obtain a meaningful dye release experiment!). There are two issues to note here. First, these observations pertain to a "strong" vesicle gel, i.e., one that has a sufficiently high modulus to maintain its integrity. Second, the hm-chitosan itself is insoluble at pH 7.1 (note that the pH inside the vesicle gel starts less than 6.5 due to the 1% acetic acid used to dissolve the chitosan initially), so it tends to form a sharp boundary when contacted with PBS.

We can now try to interpret the release profile shown in Figure 5.1b. The plot shows the cumulative dye release as a function of time. The total amount of dye encapsulated in the vesicles can be determined by analyzing the vesicle gel sample alone (for this measurement, the vesicles are typically lysed first by adding the detergent Triton X-100). The data show that even after 6000 min (100 hours), only about 40% of the dye in the vesicle gel has leaked out into the supernatant. At this point, we add some Triton X-100 to the supernatant. This molecule is expected to diffuse into the vesicle gel and begin to disrupt vesicles. If this were to occur, dye encapsulated in the vesicles would leak out, the gel would begin to degrade (since the vesicles are the crosslinks), and we should see an increase in dye release rate into the supernatant. Indeed, we observe precisely this in Figure 5.1b. The result here strongly suggests that the vesicles are indeed getting disrupted by the added Triton X-100. In turn, they imply that the vesicles remain intact throughout the dye release experiment.

The above experiment suffers from the lack of an adequate control. In other words, we would like to compare dye release from one gel with vesicles and another gel without vesicles. We could thus specifically determine the effect of vesicles on dye release. However, such a comparison is not possible with the present system *because the hm-chitosan alone does not form a gel* even at very high concentrations. It is only in the presence of vesicles that a gel is formed, with the vesicles serving as crosslinks in the gel.

An alternative therefore is to compare an hm-chitosan gel crosslinked by a different chemical moiety. For example, from the literature, mixtures of chitosan and glycerol phosphate (GP) are known to form gels at 37°C.[85] We therefore set out to prepare two gels: one with hm-chitosan crosslinked with GP (1.8% hm-chitosan and 3.6% GP) and the other with identical concentrations of hm-chitosan and GP and *also* containing EPC lipid vesicles (1.8% hm-chitosan, 3.6% GP, and 100 μL of a vesicle solution). Both gels were found to be clear and transparent at 37°C. Also, both gels were formulated to contain the same concentration of calcein dye – in the first gel, the dye was present in the gel matrix, whereas in the second case, the same amount of dye was inside the vesicles (there was no free dye outside the vesicles at the onset of the experiment).

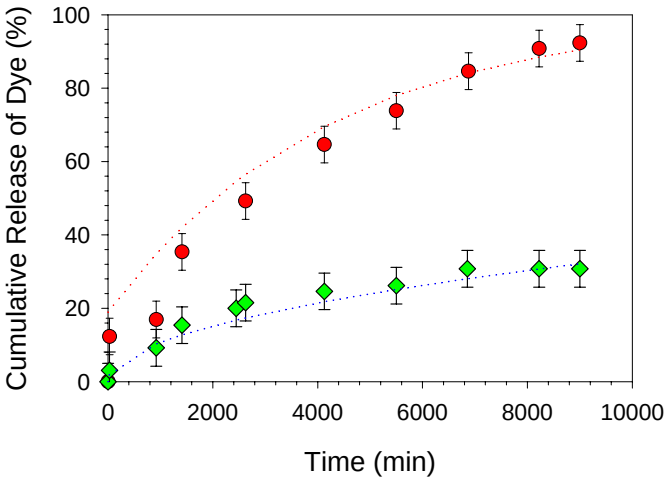

Figure 5.2. Calcein dye release profile for a control gel (1.8% hm-chitosan + 3.6% GP) (red circles), and for a vesicle gel (1.8% hm-chitosan + 3.6% GP + 100 uL lipid vesicle solution). Lines are to guide the eye.

We are now in a position to make a clear-cut comparison of the "control" gel and the vesicle gel. The results are shown in Figure 5.2. As can be seen, the release from the vesicle gel is substantially slower than from the control gel. After 9000 min (150 hours), about 90% of the dye in the control gel has leaked out, whereas only about 30% of the dye in the vesicle gel has been released into the supernatant. This provides strong evidence for a prolonged release from the vesicle gel. In turn, it confirms that the presence of two transport barriers, one from the vesicle bilayer, and the other from the gel itself, will have a net effect of slowing down the release of diffusing small molecules.

The results presented here are to be compared with a study conducted by Ruel-Gariepy et al.[85], who studied gels of chitosan-GP containing lipid vesicles. These authors also reported a slower release when vesicles were present in their gels. According to them, the release rate could be controlled either by adjusting vesicle size or composition. For example, the presence of cholesterol in the vesicle formulation was shown to substantially slow the rates of dye leakage, because cholesterol reduces the bilayer permeability. Interestingly, the gels in the above study were all made with chitosan, whereas we have used hm-chitosan. Our own experiments (data not shown) reveal that the release rate is much slower with hm-chitosan than with chitosan for an equivalent vesicle-gel formulation. We can speculate that, in the hm-chitosan case, the presence of hydrophobes allows the chains to network the vesicles, which has two effects: one, it makes the gel more sturdy; and two, it further arrests the vesicles within the gel, which might indirectly have an effect on vesicle permeability.

5.3.3. *Preparation of Capsules Loaded with Vesicles*

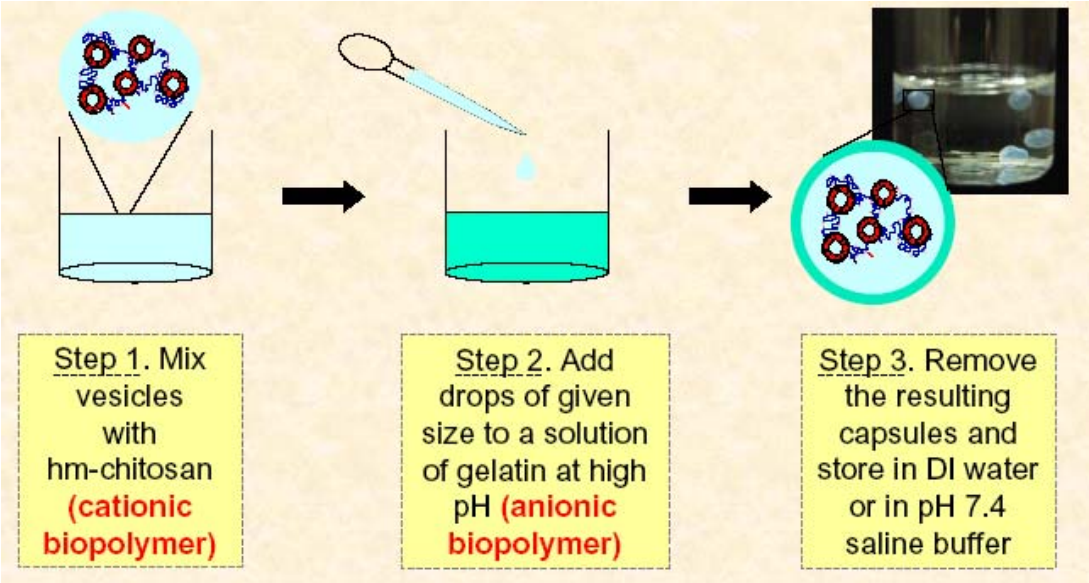

Figure 5.3. Preparation of vesicle-loaded capsules. A mixture of vesicles and cationic biopolymer (hm-chitosan) is dropped into a solution of anionic biopolymer (gelatin at high pH).

We prepare capsules by electrostatic complexation of chitosan or hm-chitosan (cationic biopolymer) and gelatin (anionic biopolymer). As illustrated by Figure 5.3, the capsules are formed when a solution of the former is dropped into a solution of the latter. The shell of the capsule is created by strong electrostatic interactions between the oppositely charged species that lead to cross-linking at the drop interface while preserving the fluid nature of the capsule interior. Note that the capsule size is controlled by the drop size and the shell thickness is a function of the droplet soak time (incubation time). For the preliminary experiments in this dissertation, we typically made large capsules (~ 3-5 mm), and a soak time of about 5 min was found to be optimal in this case. Following the soak time, the capsules were removed and

placed into either a solution of deionized water or a PBS buffer solution. The capsules formed by this process were sturdy enough to allow gentle squeezing between the fingers. Also, they remained stable for long periods of time (several weeks at least).

To make vesicle-containing capsules, the above procedure was modified. Instead of using just an hm-chitosan solution, a mixture of *vesicles and hm-chitosan* was added drop wise into a solution of gelatin. Note that mixtures of vesicles and hm-chitosan are viscous solutions or gels with a bluish tint (Chapter 3). For these capsules, we typically used a polymer concentration between 0.3 and 0.55 wt% and a vesicle concentration of 1 wt% (10 mg/mL). Note from Figure 5.3 that the capsules formed by this procedure have a bluish tint, which is a visual indicator of the presence of vesicles. The vesicle containing capsules are quite stable and retain their original size and shape for several months.

5.3.4. *Preparation of Magnetic Capsules*

We now describe the preparation of magnetic capsules for use in targeted drug delivery. The idea here is that such capsules could be manipulated and guided by a magnetic field through the bloodstream to an area of interest, such as the location of a cancerous tumor. Magnetic nanoparticles (e.g., iron oxide) are used extensively in biomedical applications, such as for contrast enhancement in MRI[86,87], and some iron oxides are approved by the Food & Drug Administration (FDA).[88] We have used commercial ferrite (γ-Fe_2O_3) nanoparticles of ca. 32 nm size in our synthesis. A dispersion of these particles (e.g., in a solution of hm-chitosan and vesicles) is then

dropped into a solution of gelatin to form the magnetic capsules (soak time ~ 2 min). Note that the ferrite particles are embedded in the interior of the capsules. The resulting capsules respond to magnetic fields as depicted in Figure 5.4. Interestingly, we find that a dispersion of ferrite particles is much more stable in the presence of hm-chitosan than chitosan. Correspondingly, the ferrite particles in hm-chitosan based capsules are relatively well-dispersed, whereas in chitosan based capsules, the particles tend to form large aggregates (Figure 5.5).

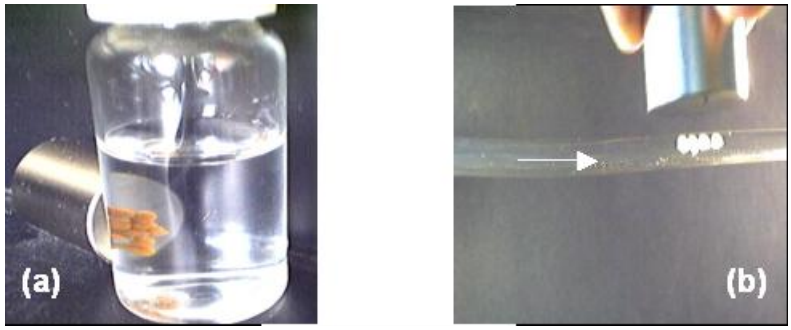

Figure 5.4. Magnetic capsules with encapsulated ferrite nanoparticles show their magnetic properties in response to a bar magnet. (a) magnet placed near capsules in a vial (b) magnet placed next to a tube in which the capsules are flowing along with the fluid (water) from left to right.

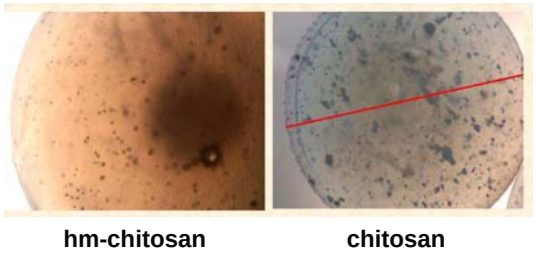

Figure 5.5. Optical micrograph of magnetic capsules showing that the ferrite nano-particles are well dispersed in capsules made with hm-chitosan (left), whereas they tend to form large aggregates in capsules made with chitosan (right).

5.3.5. *Conjugation of Antibodies to the Capsules*

In this section, we describe the synthesis of capsules with antibodies functionalized on their surface. Such capsules could be used for targeted drug delivery, for example to cancerous tumors.[89-91] Cancerous tumors are known to overexpress particular antigens, which may thus be targeted for delivery of toxic drugs directly to the tumor and nowhere else.[92] Such targeting has been attempted since 1975 and a number of such antibody-coated drug delivery vehicles have been approved by the FDA.[93]

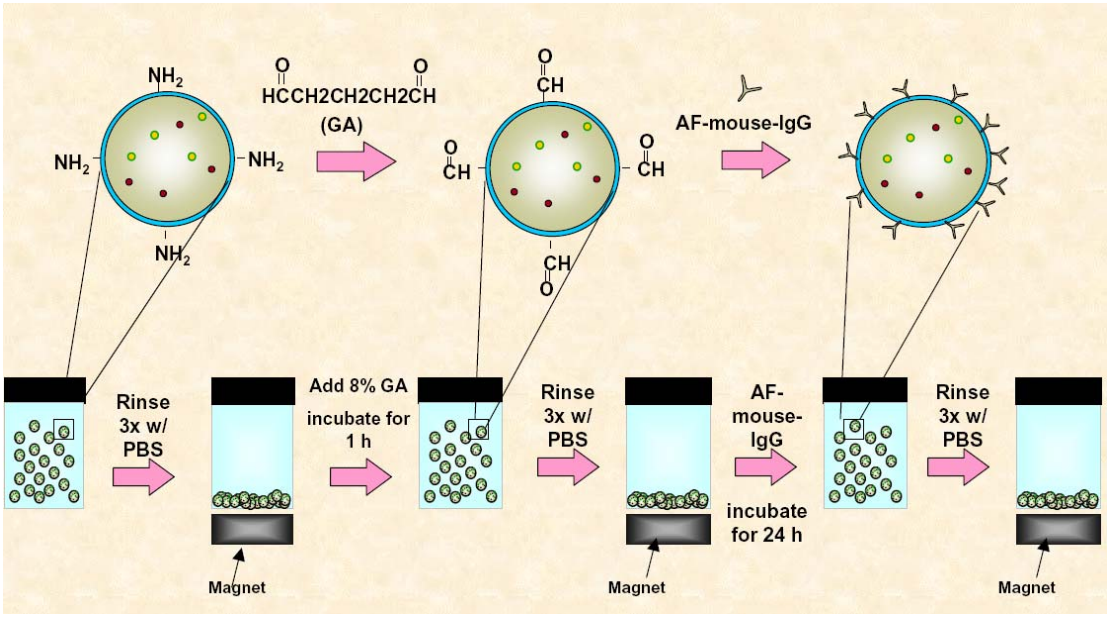

Figure 5.6. Schematic showing the steps involved in the attachment of antibodies to chitosan-based capsules.

Here, to demonstrate a proof-of-concept, we study the attachment of fluorescently-labeled mouse IgG antibodies onto the surface of magnetic biopolymer capsules. For this synthesis (Figure 5.6), we exploit the fact that the capsules bear a

number of amine groups from the chitosan. Glutaraldehyde is used as a bifunctional linker, which attaches to a amine from chitosan on the one hand and to an amine from the antibody on the other hand. As shown in Figure 5.6, the magnetic response of the capsules is used to separate them after each step in the process. Interestingly, the capsules originally have a brown color due to the ferrite nanoparticles, but after attaching the antibodies they become pink or red. This is a visual indication that antibodies are successfully attached on the capsule surface.

To demonstrate successful functionalization, the antibody-bearing capsules were brought in contact with their corresponding antigen (FL-anti-mouse-IgG). After washing several times with buffer, the capsules were examined under fluorescence microscopy. Fluorescence images of these capsules simultaneously show both a red color (from the AF-mouse-IgG) and a green color (from the FL-anti-mouse-IgG) (Figure 5.7). This result confirms successful binding of antigen to antibodies on the capsule surface. The above procedure can be repeated with any desired antibody and would thus allow these capsules to be used for targeted drug delivery applications.

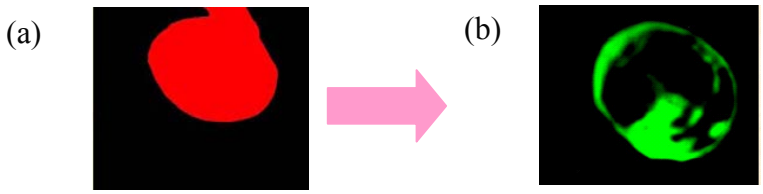

Figure 5.7. Fluorescence microscopy shows that antibodies conjugated on the surface of chitosan capsules are bound to antigens. The capsule shows a red color (a) due to the AF-mouse-IgG antibodies on its surface, and simultaneously a non-uniform green color (b) from the FL-anti-mouse-IgG antigens bound to the above antibodies.

5.3.6. *Dye Release from Vesicle-Loaded Capsules*

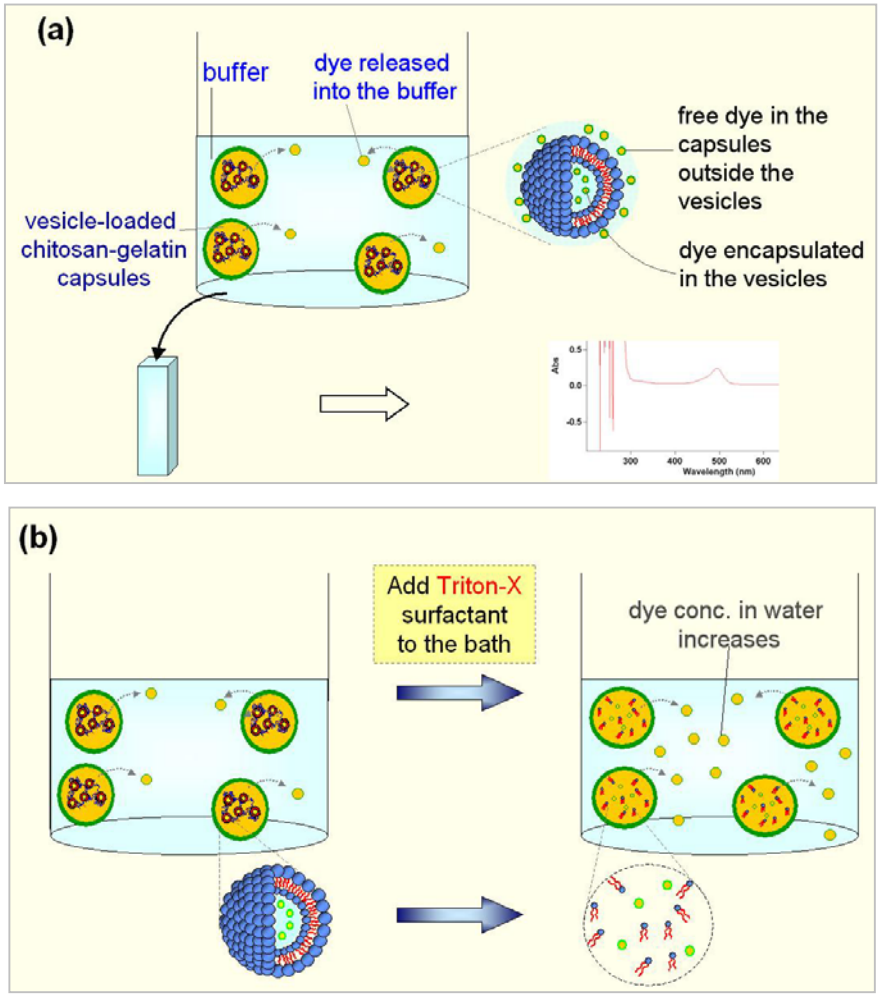

Figure 5.8. Schematics of dye release experiments with vesicle-loaded biopolymer capsules (a) Capsules are immersed in a bath of buffer and the dye concentration in the bath is monitored. (b) The addition of Triton-X to the bath causes the vesicles in the capsules to break down into micelles.

In this final section, we study dye release from vesicle-loaded capsules, with calcein serving as a model hydrophilic dye. Capsules for these studies were prepared as follows. First, a solution containing 1 wt% surfactant vesicles (70/30 mass ratio of CTAT/SDBS), 0.55 wt% hm-chitosan, and 0.5 mM calcein was prepared. After centrifuging to remove bubbles, drops of this solution were added into a 0.5 wt%

solution of gelatin at pH around 12. The resulting capsules were removed and placed into a bath of PBS buffer (Figure 5.8a). In addition, a control experiment was conducted with capsules that were identical in all respects (same amounts of hm-chitosan, gelatin and CF), except that they did not contain any vesicles. These control capsules were also placed in a second bath of PBS buffer. In each case, aliquots of buffer medium were removed at different time intervals and analyzed by UV-Vis spectrometry to obtain the dye concentration as a function of time.

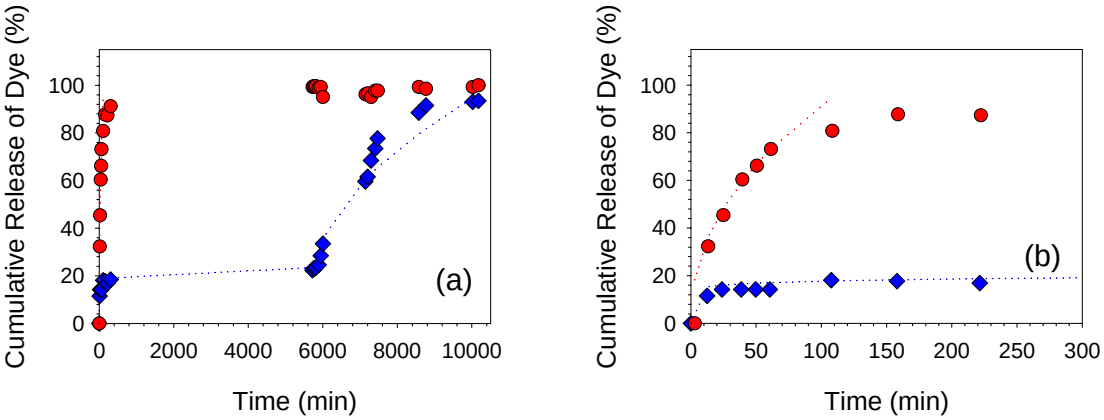

Figure 5.9. Dye release profiles from vesicle-loaded capsules (blue diamonds) and the control (vesicle-free) capsules (red circles): (a) Results over a period of 10000 minutes. At the 6000 min mark, the detergent Triton-X 100 is added to each bath. (b) Close-up of the release over the first 300 min, showing that most of the dye in the control capsules is released over this period. The dotted lines are fits to eq. 5.1.

Dye release profiles are shown in Figure 5.9 for both the control capsules as well as the vesicle-loaded capsules. Note that the release of dye is very rapid from the control capsules, with more than 80% of the dye being released within the first 200 min. On the other hand, the release from vesicle-loaded capsules is much slower and only about 20% of the dye is released from these capsules even after 6000 min. At this point, we added the detergent Triton-X 100 to the bath. This detergent will

diffuse through the capsule wall and destabilize the vesicles in the interior of the capsules, as shown in Figure 5.8b. As shown in the figure, the vesicles will be transformed into micelles, and thereby, the hydrophilic drug in the vesicles will be released within the capsules. This free dye will then leak out through the capsule shell and into the bath, thereby increasing the dye concentration. Indeed, our results (Figure 5.9a) show that the dye release accelerates after we add Triton-X 100 to the bath. These observations also confirm that the vesicles are present intact in the capsules before we add the detergent.

To obtain further insight into the dye release behavior, we fit our release profiles to the empirical relation below, devised originally by Ritger and Peppas[94]:

$$\frac{M_t}{M_\infty} = kt^n$$

Here M_t is the cumulative amount of dye released into the bath at time t and M_∞ is the total amount of dye that gets released. The variables in this equation are the power law index n and the constant k. The key variable is n, and the transport process is considered to be diffusion-controlled (Fickian transport) if $n = 0.5$. On the other hand, if $0.5 < n < 1$, the process is deemed non-Fickian or anomalous transport, and finally if $n = 1$, it is referred to as zero-order or relaxation-controlled transport.[95] This equation works well only in the initial portion of the release profiles, and so we have fit the data over the first 300 min (Figure 5.9b). The best-fit value of n for the control capsules was found to be 0.46, while for the vesicle-loaded capsules, n was 0.07. After the addition of Triton-X 100, the n value for the vesicle-loaded capsules

increased to 0.56. Note that a value close to 0.5 is found for both the control capsules as well as the vesicle-loaded capsules after vesicle destabilization. This result implies that in both these cases, the transport process is approximately diffusion-limited. The lower value of 0.07 for the vesicle-loaded capsules indicates a combination of transport barriers from the vesicle bilayer and from the capsule shell. Further experiments are under way to investigate these processes in more detail. In summary, the data show that vesicle-loaded capsules can be used for extended release of drugs or other molecules over periods of even weeks or months. The release rate can be accelerated if the vesicles inside the capsules are disrupted by an external stimulus.

5.4. Conclusions

In this Chapter, we have studied the release of dye from vesicle gels and vesicle-loaded capsules. Comparison of the dye release profiles from vesicle-loaded gels and capsules and those obtained from control gels and capsules reveals that the release rate is slowed down appreciably when vesicles are included in the formulation. The results indicate that vesicle-containing gels and capsules could be used for the sustained delivery of small-molecular weight hydrophilic compounds. Additionally, in this chapter, we have described how to impart targeting capabilities to vesicle-loaded capsules. These include targeting by magnetic fields due to embedded magnetic ferrite nanoparticles, and targeting by biomolecular interactions via antibodies functionalized to the capsule surface. Thus, we envision applications for these hybrid capsules in targeted drug delivery as well.

Chapter 6

Conclusions and Recommendations

6.1. Conclusions

We have studied the interactions between an associating biopolymer (hm-chitosan) and vesicles (Chapters 3, 4) and the potential use of this system in drug delivery and controlled release applications (Chapter 5). We used two different types of vesicles: (1) surfactant vesicles made by mixing CTAT/SDBS in a 70/30 weight ratio; and (2) egg-yolk phosphatidylcholine (EPC) lipid vesicles. In both cases, we found that gels are formed when hm-chitosan is mixed with the vesicles. Interestingly, these gels have sufficient yield stresses such that they do not flow upon inverting their vials. The presence of vesicles in the gels was confirmed by visual observations (i.e., the bluish color of the gels) as well as by SANS and cryo-TEM experiments. Based on these findings, we postulated that the likely structure of these gels is a network of vesicles connected by associating polymer chains, with the hydrophobes on the polymer inserted into the vesicle bilayers.

A more in-depth study using SANS and cryo-TEM (Chapter 4) revealed that upon addition of low amounts of the hm-chitosan, the vesicles re-organized into smaller entities so as to present more surface area for interaction with the polymer hydrophobes. At higher polymer:vesicle ratios, the addition of the hm-chitosan

caused some of the originally unilamellar vesicles (ULVs) to fuse into bilamellar vesicles (BLVs). A co-existence of ULVs and BLVs was directly visualized by cryo-TEM. Moreover, this co-existence gave rise to a striking pattern in SANS with multiple peaks, and we were able to model this SANS data to corroborate such a vesicular co-existence. Also, SANS data taken on the same sample after more than a year indicated that the co-existence of ULVs and BLVs was a stable phenomenon.

In Chapter 5, we conducted dye release studies using vesicle + hm-chitosan gels made using either surfactant vesicles or lipid vesicles (liposomes). Vesicle gels retained their stability when placed in contact with a buffer (PBS) solution, which indicates that *in vivo* experiments are possible with these gels. Also, the release rate of dye from the gel into the buffer was significantly slower when the dye was encapsulated within the vesicles. This result suggested that the combination of transport resistances from the vesicle bilayer and the polymer matrix was effective in suppressing the release of dye.

Chapter 5 also reported our experiments with a second type of structure, i.e., biopolymer capsules. We made capsules by contacting chitosan solution droplets with a solution of an anionic biopolymer or surfactant. Polyelectrolyte complexation leads to cross-linking at the drop interface while preserving fluidity inside the capsule. We then modified the capsule structure so as to make vesicle-loaded capsules. Dye release experiments again indicated that vesicle containing capsules released dye much slower than control (vesicle-free) capsules. Additionally, the release rate could

be accelerated if the disruption of vesicles could be triggered by external stimuli. These results were encouraging and they suggest that our hybrid vesicle-loaded capsules may be useful for sustained release of drugs or other molecules.

Finally, in Chapter 5, we also investigated the preparation of capsules suitable for targeted drug release. The simplicity of the capsule forming process allowed us to incorporate ferrite nanoparticles together with the vesicles into the capsules. Capsules containing magnetic nanoparticles can be targeted to a desired location using a magnetic field. Also, we also showed how we can easily functionalize antibodies onto the capsule surface using a bifunctional linker such as glutaraldehyde. The antibodies permit the capsules to be used for biomolecular targeting, such as to corresponding antigens present on cancer cells.

6.2. Recommendations for Future Work

Study of the Interactions Between Liposomes and Associating Biopolymers

In our study of the interactions between *surfactant vesicles* and hm-chitosan, SANS and cryo-TEM were proven to be valuable tools to understand the structure inside the resulting gels as well as the structural changes that vesicles undergo upon adding the polymer. It would be interesting to repeat the above SANS + cryo-TEM studies with *lipid vesicles* (liposomes) and hm-chitosan. For this future study, N-acyl chitosan should be used in addition to the hm-chitosan mentioned throughout this dissertation. N-acyl chitosan is known for its blood compatibility, biodegradability and ease of preparation.[35,96] In addition to hydrophobically modified chitosans, it may

be worthwhile to study the interactions between liposomes and recently developed hydrophobically modified alginate.[97] Alginate capsules have found widespread use and a variant of the capsules wherein vesicles are added may rapidly result in a commercially available product.

In Vivo Studies with Vesicle Gels and Vesicle-Loaded Capsules

In vivo studies of vesicle loaded gels and capsules can be done in the future. To avoid being ejected from the body through the RES, the capsule size can be further decreased using a new ink-jet technology[98]. Targetable capsules can be studied for the treatment of cancer. Targeting ability of magnetic capsules can be evaluated *in vivo* using magnetic resonance imaging (MRI). For biomolecular targeting, the capsule surface will have to be modified with the correct antigens that are known to be present on the exterior of tumor cells.

For these future release studies, different types of lipid vesicles may be used. In particular, it would be interesting to work with *hyperthermal liposomes*, which can be induced to trigger by changing temperature.[5] An example of such a temperature-sensitive formulation is the mixture of mixture of the lipids DPPC (1,2-dipalmitoyl-sn-glycero-3-phosphocholine), MPPC (1-palmitoyl-2-hydroxy-snglycero-3-phospho-choline), and DSPE-PEG-2000 (1,2-distearoyl-snglycero-3-phosphoethanolamine-N-polyethylene glycol 2000).[5] Other possibilities for triggered release include that catalyzed by enzymes such as phospholipase A_2 (this enzyme could be encapsulated in capsules along with vesicles and would slowly degrade the vesicles).[76]

Vesicle-loaded capsules can also be evaluated for the release of large macromolecules (e.g., proteins). For example, fluorescein isothiocyanate (FITC)-labeled bovine serum albumin (BSA), FITC-horseradish peroxidase (HRP), and various growth factors including vascular endothelial growth factor (VEGF), basic fibroblast growth factor (bFGF), epidermal growth factor (EGF) and bone morphogenetic protein (BMP) can be encapsulated in vesicle-loaded capsules and their release profiles studied.

Giant Vesicles

Finally, it will be interesting to study the addition of hm-chitosan to giant vesicles. These vesicles can be prepared by the electroformation technique[21] and they can be visualized using optical microscopy. The advantage of working with giant vesicles is that it may be possible to directly observe changes in vesicle structure when the hm-chitosan is added. For example, the addition of hm-chitosan may break large vesicles into smaller ones.[99] Phenomena such as vesicle budding or pearling may also be induced by the polymer.[100] The role of hydrophobes can be elucidated by comparing the hm-chitosan and the unmodified chitosan. Using fluorescent tags, it may be possible to show that the hydrophobic moieties are indeed anchored inside vesicle bilayers.

References

[1] Lasic, D. D. *Liposomes: From Physics to Applications*; Elsevier: Amsterdam, 1993.

[2] Kaler, E. W.; Murthy, A. K.; Rodriguez, B. E.; Zasadzinski, J. A. N. "Spontaneous Vesicle Formation in Aqueous Mixtures of Single-Tailed Surfactants." *Science* **1989**, *245*, 1371-1374.

[3] Discher, D. E.; Eisenberg, A. "Polymer vesicles." *Science* **2002**, *297*, 967-973.

[4] *Liposomes: Rational Design*; Janoff, A. S., Ed.; Marcel Dekker: New York, 1999.

[5] Needham, D.; Anyarambhatla, G.; Kong, G.; Dewhirst, M. W. "A new temperature-sensitive liposome for use with mild hyperthermia: Characterization and testing in a human tumor xenograft model." *Cancer Research* **2000**, *60*, 1197-1201.

[6] Managit, C.; Kawakami, S.; Nishikawa, M.; Yamashita, F.; Hashida, M. "Targeted and sustained drug delivery using PEGylated galactosylated liposomes." *International Journal of Pharmaceutics* **2003**, *266*, 77-84.

[7] Torchilin, V. P. "Recent advances with liposomes as pharmaceutical carriers." *Nature Reviews Drug Discovery* **2005**, *4*, 145-160.

[8] Lasic, D. D.; Needham, D. "The "Stealth" liposome: A prototypical biomaterial." *Chemical Reviews* **1995**, *95*, 2601-2628.

[9] Gabizon, A.; Papahadjopoulos, D. "Liposome Formulations with Prolonged Circulation Time in Blood and Enhanced Uptake by Tumors." *Proceedings of the National Academy of Sciences of the United States of America* **1988**, *85*, 6949-6953.

[10] Loyen, K.; Iliopoulos, I.; Audebert, R.; Olsson, U. "Reversible Thermal Gelation in Polymer Surfactant Systems - Control of the Gelation Temperature." *Langmuir* **1995**, *11*, 1053-1056.

[11] Meier, W.; Hotz, J.; Gunther Ausborn, S. "Vesicle and cell networks: Interconnecting cells by synthetic polymers." *Langmuir* **1996**, *12*, 5028-5032.

[12] Marques, E. F.; Regev, O.; Khan, A.; Miguel, M. D.; Lindman, B. "Interactions between catanionic vesicles and oppositely charged poly electrolytes-phase behavior and phase structure." *Macromolecules* **1999**, *32*, 6626-6637.

[13] Ashbaugh, H. S.; Boon, K.; Prud'homme, R. K. "Gelation of "catanionic" vesicles by hydrophobically modified polyelectrolytes." *Colloid and Polymer Science* **2002**, *280*, 783-788.

[14] Antunes, F. E.; Marques, E. F.; Gomes, R.; Thuresson, K.; Lindman, B.; Miguel, M. G. "Network formation of catanionic vesicles and oppositely charged polyelectrolytes. Effect of polymer charge density and hydrophobic modification." *Langmuir* **2004**, *20*, 4647-4656.

[15] Berger, J.; Reist, M.; Mayer, J. M.; Felt, O.; Gurny, R. "Structure and interactions in chitosan hydrogels formed by complexation or aggregation for biomedical applications." *European Journal of Pharmaceutics and Biopharmaceutics* **2004**, *57*, 35-52.

[16] Ohkawa, K.; Kitagawa, T.; Yamamoto, H. "Preparation and characterization of chitosan-gellan hybrid capsules formed by self-assembly at an aqueous solution interface." *Macromolecular Materials and Engineering* **2004**, *289*, 33-40.

[17] Peniche, C.; Arguelles-Monal, W.; Peniche, H.; Acosta, N. "Chitosan: An attractive biocompatible polymer for microencapsulation." *Macromolecular Bioscience* **2003**, *3*, 511-520.

[18] Evans, D. F.; Wennerstrom, H. *The Colloidal Domain: Where Physics, Chemistry, Biology, and Technology Meet*; Wiley-VCH: New York, 2001.

[19] Israelachvili, J. N. *Intermolecular and Surface Forces*; Academic Press: New York, 1992.

[20] Avanti_Polar_Lipids. http://www.avantilipids.com/PreparationOfLiposomes.html. **2004**.

[21] *Giant Vesicles*; Luisi, P. L.; Walde, P., Eds.; Wiley: New York, 2000.

[22] Annable, T.; Buscall, R.; Ettelaie, R.; Whittlestone, D. "The Rheology of Solutions of Associating Polymers - Comparison of Experimental Behavior with Transient Network Theory." *Journal of Rheology* **1993**, *37*, 695-726.

[23] Desbrieres, J.; Martinez, C.; Rinaudo, M. "Hydrophobic derivatives of chitosan: Characterization and rheological behaviour." *International Journal of Biological Macromolecules* **1996**, *19*, 21-28.

[24] Menchen, S.; Johnson, B.; Winnik, M. A.; Xu, B. "Flowable networks as equilibrium DNA sequencing media in capillary columns." *Chemistry of Materials* **1996**, *8*, 2205-2208.

[25] Alberts, B. et. al. *Molecular Biology of the Cell.* Available online at http://www.ncbi.nlm.nih.gov/books/ Garland Publishing: New York, 1994.

[26] Skjak-Braek, G.; Anthonsen, T.; Sandford, P. *Chitin and Chitosan: Sources, Chemistry, Biochemistry, Physical Properties, and Applications*; Elsevier: London, 1988.

[27] Uchegbu, I. F.; Schatzlein, A. G.; Tetley, L.; Gray, A. I.; Sludden, J.; Siddique, S.; Mosha, E. "Polymeric chitosan-based vesicles for drug delivery." *Journal of Pharmacy and Pharmacology* **1998**, *50*, 453-458.

[28] Illum, L. "Chitosan and its use as a pharmaceutical excipient." *Pharmaceutical Research* **1998**, *15*, 1326-1331.

[29] Miyazaki, S.; Ishii, K.; Nadai, T. "The Use of Chitin and Chitosan as Drug Carriers." *Chemical & Pharmaceutical Bulletin* **1981**, *29*, 3067-3069.

[30] Kumar, M. "A review of chitin and chitosan applications." *Reactive & Functional Polymers* **2000**, *46*, 1-27.

[31] Chen, T. H.; Kumar, G.; Harris, M. T.; Smith, P. J.; Payne, G. F. "Enzymatic grafting of hexyloxyphenol onto chitosan to alter surface and rheological properties." *Biotechnology and Bioengineering* **2000**, *70*, 564-573.

[32] Aberg, C. M.; Chen, T. H.; Olumide, A.; Raghavan, S. R.; Payne, G. F. "Enzymatic grafting of peptides from casein hydrolysate to chitosan. potential for value-added byproducts from food-processing wastes." *Journal of Agricultural and Food Chemistry* **2004**, *52*, 788-793.

[33] Bernkop-Schnurch, A. "Chitosan and its derivatives: potential excipients for peroral peptide delivery systems." *International Journal of Pharmaceutics* **2000**, *194*, 1-13.

[34] Yalpani, M.; Hall, L. D. "Some Chemical and Analytical Aspects of Polysaccharide Modifications.3. Formation of Branched-Chain, Soluble Chitosan Derivatives." *Macromolecules* **1984**, *17*, 272-281.

[35] Hirano, S.; Ohe, Y.; Ono, H. "Selective N-Acylation of Chitosan." *Carbohydrate Research* **1976**, *47*, 315-320.

[36] Domszy, J. G.; Roberts, G. A. F. "Evaluation of Infrared Spectroscopic Techniques for Analyzing Chitosan." *Makromolekulare Chemie-Macromolecular Chemistry and Physics* **1985**, *186*, 1671-1677.

[37] Le Tien, C.; Lacroix, M.; Ispas-Szabo, P.; Mateescu, M. A. "N-acylated chitosan: hydrophobic matrices for controlled drug release." *Journal of Controlled Release* **2003**, *93*, 1-13.

[38] Macosko, C. W. *Rheology: Principles, Measurements and Applications*; VCH Publishers: New York, 1994.

[39] *Neutron, X-Ray and Light Scattering: Introduction to an Investigative Tool for Colloidal and Polymeric Systems*; Zemb, T.; Lindner, P., Eds.; Elsevier: Amsterdam, 1991.

[40] Brown, W. *Dynamic Light Scattering: The Method and some Applications*; Clarendon Press: Oxford, 1993.

[41] Kim, M. K.; Chung, S. J.; Lee, M. H.; Cho, A. R.; Shim, C. K. "Targeted and sustained delivery of hydrocortisone to normal and stratum corneum-removed skin without enhanced skin absorption using a liposome gel." *Journal of Controlled Release* **1997**, *46*, 243-251.

[42] Kevelam, J.; vanBreemen, J. F. L.; Blokzijl, W.; Engberts, J. "Polymer-surfactant interactions studied by titration microcalorimetry: Influence of polymer hydrophobicity, electrostatic forces, and surfactant aggregational state." *Langmuir* **1996**, *12*, 4709-4717.

[43] Murphy, A.; Hill, A.; Vincent, B. "The effect of cationic polyelectrolytes, containing terminal hydrophobic anchors, on the stability of vesicles of dioctadecyldimethylammonium chloride in calcium chloride solutions." *Berichte Der Bunsen-Gesellschaft-Physical Chemistry Chemical Physics* **1996**, *100*, 963-971.

[44] Regev, O.; Marques, E. F.; Khan, A. "Polymer-induced structural effects on catanionic vesicles: Formation of faceted vesicles, disks, and cross-links." *Langmuir* **1999**, *15*, 642-645.

[45] Kjoniksen, A. L.; Iversen, C.; Nystrom, B.; Nakken, T.; Palmgren, O. "Light scattering study of semidilute aqueous systems of chitosan and hydrophobically modified chitosans." *Macromolecules* **1998**, *31*, 8142-8148.

[46] Esquenet, C.; Terech, P.; Boue, F.; Buhler, E. "Structural and rheological properties of hydrophobically modified polysaccharide associative networks." *Langmuir* **2004**, *20*, 3583-3592.

[47] Koehler, R. D.; Raghavan, S. R.; Kaler, E. W. "Microstructure and dynamics of wormlike micellar solutions formed by mixing cationic and anionic surfactants." *Journal of Physical Chemistry B* **2000**, *104*, 11035-11044.

[48] *Small-Angle X-Ray Scattering*; Glatter, O.; Kratky, O., Eds.; Academic Press: New York, 1982.

[49] Li, H.; Yu, G. E.; Price, C.; Booth, C.; Hecht, E.; Hoffmann, H. "Concentrated aqueous micellar solutions of diblock copoly(oxyethylene/oxybutylene) E(41)B(8): A study of phase behavior." *Macromolecules* **1997**, *30*, 1347-1354.

[50] Winter, H. H.; Chambon, F. "Analysis of Linear Viscoelasticity of a Cross-Linking Polymer at the Gel Point." *Journal of Rheology* **1986**, *30*, 367-382.

[51] McKelvey, C. A.; Kaler, E. W.; Zasadzinski, J. A.; Coldren, B.; Jung, H. T. "Templating hollow polymeric spheres from catanionic equilibrium vesicles: Synthesis and characterization." *Langmuir* **2000**, *16*, 8285-8290.

[52] Milner, S. T.; Witten, T. A. "Bridging Attraction by Telechelic Polymers." *Macromolecules* **1992**, *25*, 5495-5503.

[53] Lipowsky, R. "Flexible membranes with anchored polymers." *Colloids and Surfaces A-Physicochemical and Engineering Aspects* **1997**, *128*, 255-264.

[54] Filali, M.; Ouazzani, M. J.; Michel, E.; Aznar, R.; Porte, G.; Appell, J. "Robust phase behavior of model transient networks." *Journal of Physical Chemistry B* **2001**, *105*, 10528-10535.

[55] Jung, H. T.; Coldren, B.; Zasadzinski, J. A.; Iampietro, D. J.; Kaler, E. W. "The origins of stability of spontaneous vesicles." *Proceedings of the National Academy of Sciences of the United States of America* **2001**, *98*, 1353-1357.

[56] Jung, H. T.; Lee, S. Y.; Kaler, E. W.; Coldren, B.; Zasadzinski, J. A. "Gaussian curvature and the equilibrium among bilayer cylinders, spheres, and discs." *Proceedings of the National Academy of Sciences of the United States of America* **2002**, *99*, 15318-15322.

[57] Gradzielski, M.; Muller, M.; Bergmeier, M.; Hoffmann, H.; Hoinkis, E. "Structural and macroscopic characterization of a gel phase of densely packed monodisperse, unilamellar vesicles." *Journal of Physical Chemistry B* **1999**, *103*, 1416-1424.

[58] Panizza, P.; Roux, D.; Vuillaume, V.; Lu, C. Y. D.; Cates, M. E. "Viscoelasticity of the onion phase." *Langmuir* **1996**, *12*, 248-252.

[59] Nallet, F.; Laversanne, R.; Roux, D. "Modeling X-Ray or Neutron-Scattering Spectra of Lyotropic Lamellar Phases - Interplay between Form and Structure Factors." *Journal De Physique I* **1993**, *3*, 487-502.

[60] Castro-Roman, F.; Porte, G.; Ligoure, C. "Renormalization of Helfrich's interactions between fluid membranes in a lyotropic lamellar phase by addition of amphiphilic." *Physical Review Letters* **1999**, *82*, 109-112.

[61] Yang, B. S.; Lal, J.; Richetti, P.; Marques, C. M.; Russel, W. B.; Prud'homme, R. K. "Interaction of hydrophobically modified polymers." *Langmuir* **2001**, *17*, 5834-5841.

[62] Danino, D.; Talmon, Y.; Zana, R. "Cryo-TEM of thread-like micelles: on-the-grid microstructural transformations induced during specimen preparation." *Colloids and Surfaces A-Physicochemical and Engineering Aspects* **2000**, *169*, 67-73.

[63] Nieh, M. P.; Glinka, C. J.; Krueger, S.; Prosser, R. S.; Katsaras, J. "SANS study on the effect of lanthanide ions and charged lipids on the morphology of phospholipid mixtures." *Biophysical Journal* **2002**, *82*, 2487-2498.

[64] Yang, B. S.; Lal, J.; Kohn, J.; Huang, J. S.; Russel, W. B.; Prud'homme, R. K. "Interaction of surfactant lamellar phase and a strictly alternating comb-graft amphiphilic polymer based on PEG." *Langmuir* **2001**, *17*, 6692-6698.

[65] Harrington, K. J.; Lewanski, C.; Northcote, A. D.; Whittaker, J.; Peters, A. M.; Vile, R. G.; Stewart, J. S. W. "Phase II study of pegylated liposomal doxorubicin (Caelyx (TM)) as induction chemotherapy for patients with squamous cell cancer of the head and neck." *European Journal Of Cancer* **2001**, *37*, 2015-2022.

[66] Woodle, M. C.; Lasic, D. D. "Sterically Stabilized Liposomes." *Biochimica Et Biophysica Acta* **1992**, *1113*, 171-199.

[67] Du, H.; Chandaroy, P.; Hui, S. W. "Grafted poly-(ethylene glycol) on lipid surfaces inhibits protein adsorption and cell adhesion." *Biochimica Et Biophysica Acta-Biomembranes* **1997**, *1326*, 236-248.

[68] Misra, A.; Ganesh, S.; Shahiwala, A.; Shah, S. P. "Drug delivery to the central nervous system: a review." *Journal Of Pharmacy And Pharmaceutical Sciences* **2003**, *6*, 252-273.

[69] Weiner, A. L.; Carpentergreen, S. S.; Soehngen, E. C.; Lenk, R. P.; Popescu, M. C. "Liposome Collagen Gel Matrix - a Novel Sustained Drug Delivery System." *Journal of Pharmaceutical Sciences* **1985**, *74*, 922-925.

[70] Gabrijelcic, V.; Sentjurc, M. "Influence of Hydrogels on Liposome Stability and on the Transport of Liposome-Entrapped Substances into the Skin." *International Journal of Pharmaceutics* **1995**, *118*, 207-212.

[71] Pavelic, Z.; Skalko-Basnet, N.; Schubert, R. "Liposomal gels for vaginal drug delivery." *International Journal of Pharmaceutics* **2001**, *219*, 139-149.

[72] DiTizio, V.; Karlgard, C.; Lilge, L.; Khoury, A. E.; Mittelman, M. W.; DiCosmo, F. "Localized drug delivery using crosslinked gelatin gels containing liposomes: Factors influencing liposome stability and drug release." *Journal of Biomedical Materials Research* **2000**, *51*, 96-106.

[73] Morris, W.; Steinhoff, M. C.; Russell, P. K. "Potential of Polymer Microencapsulation Technology for Vaccine Innovation." *Vaccine* **1994**, *12*, 5-11.

[74] Hoffman, A. S. "Hydrogels for biomedical applications." *Advanced Drug Delivery Reviews* **2002**, *54*, 3-12.

[75] Lee, K. Y.; Mooney, D. J. "Hydrogels for tissue engineering." *Chemical Reviews* **2001**, *101*, 1869-1879.

[76] Kibat, P. G.; Igari, Y.; Wheatley, M. A.; Eisen, H. N.; Langer, R. "Enzymatically Activated Microencapsulated Liposomes Can Provide Pulsatile Drug Release." *FASEB Journal* **1990**, *4*, 2533-2539.

[77] Wheatley, M. A.; Langer, R. "Particles as Drug Delivery Systems." *Particle Science Technology* **1987**, *5*, 53-65.

[78] Cohen, S.; Bernstein, H.; Hewes, C.; Chow, M.; Langer, R. "The Pharmacokinetics of, and Humoral Responses to, Antigen Delivered by Microencapsulated Liposomes." *Proceedings of the National Academy of Sciences of the United States of America* **1991**, *88*, 10440-10444.

[79] Machluf, M.; Regev, O.; Peled, Y.; Kost, J.; Cohen, S. "Characterization of microencapsulated liposome systems for the controlled delivery of liposome-associated macromolecules." *Journal of Controlled Release* **1997**, *43*, 35-45.

[80] Machluf, M.; Apte, R. N.; Regev, O.; Cohen, S. "Enhancing the immunogenicity of liposomal hepatitis B surface antigen (HBsAg) by controlling its delivery from polymeric microspheres." *Journal of Pharmaceutical Sciences* **2000**, *89*, 1550-1557.

[81] Dhoot, N. O.; Wheatley, M. A. "Microencapsulated Liposomes in controlled drug delivery: Strategies to modulate drug release and eliminate the burst effect." *Journal of Pharmaceutical Sciences* **2003**, *92*, 679-689.

[82] Ramadas, M.; Paul, W.; Dileep, K. J.; Anitha, Y.; Sharma, C. P. "Lipoinsulin encapsulated alginate-chitosan capsules: intestinal delivery in diabetic rats." *Journal of Microencapsulation* **2000**, *17*, 405-411.

[83] Szoka, F.; Olson, F.; Heath, T.; Vail, W.; Mayhew, E.; Papahadjopoulos, D. "Preparation of Unilamellar Liposomes of Intermediate Size (0.1-0.2-Mumm) by a Combination of Reverse Phase Evaporation and Extrusion through Polycarbonate Membranes." *Biochimica Et Biophysica Acta* **1980**, *601*, 559-571.

[84] Koh, I. Ph.D. Dissertation, University of Maryland, 2005.

[85] Ruel-Gariepy, E.; Leclair, G.; Hildgen, P.; Gupta, A.; Leroux, J. C. "Thermosensitive chitosan-based hydrogel containing liposomes for the delivery of hydrophilic molecules." *Journal of Controlled Release* **2002**, *82*, 373-383.

[86] Weissleder, R.; Elizondo, G.; Wittenberg, J.; Rabito, C. A.; Bengele, H. H.; Josephson, L. "Ultrasmall Superparamagnetic Iron-Oxide - Characterization of a New Class of Contrast Agents for Mr Imaging." *Radiology* **1990**, *175*, 489-493.

[87] Lewin, M.; Carlesso, N.; Tung, C. H.; Tang, X. W.; Cory, D.; Scadden, D. T.; Weissleder, R. "Tat peptide-derivatized magnetic nanoparticles allow in vivo tracking and recovery of progenitor cells." *Nature Biotechnology* **2000**, *18*, 410-414.

[88] Semelka, R. C.; Helmberger, T. K. G. "Contrast agents for MR imaging of the liver." *Radiology* **2001**, *218*, 27-38.

[89] Stolnik, S.; Dunn, S. E.; Garnett, M. C.; Davies, M. C.; Coombes, A. G. A.; Taylor, D. C.; Irving, M. P.; Purkiss, S. C.; Tadros, T. F.; Davis, S. S.; Illum, L. "Surface Modification of Poly(Lactide-Co-Glycolide) Nanospheres by Biodegradable Poly(Lactide)-Poly(Ethylene Glycol) Copolymers." *Pharmaceutical Research* **1994**, *11*, 1800-1808.

[90] Hawley, A. E.; Illum, L.; Davis, S. S. "Preparation of biodegradable, surface engineered PLGA nanospheres with enhanced lymphatic drainage and lymph node uptake." *Pharmaceutical Research* **1997**, *14*, 657-661.

[91] Storm, G.; Belliot, S. O.; Daemen, T.; Lasic, D. D. "Surface Modification of Nanoparticles to Oppose Uptake by the Mononuclear Phagocyte System." *Advanced Drug Delivery Reviews* **1995**, *17*, 31-48.

[92] Glennie, M. J.; van de Winkel, J. G. J. "Renaissance of cancer therapeutic antibodies." *Drug Discovery Today* **2003**, *8*, 503-510.

[93] Brannon-Peppas, L.; Blanchette, J. O. "Nanoparticle and targeted systems for cancer therapy." *Advanced Drug Delivery Reviews* **2004**, *56*, 1649-1659.

[94] Ritger, P. L.; Peppas, N. A. "Transport of Penetrants in the Macromolecular Structure of Coals.4. Models for Analysis of Dynamic Penetrant Transport." *Fuel* **1987**, *66*, 815-826.

[95] Agnihotri, S. A.; Aminabhavi, T. M. "Controlled release of clozapine through chitosan microparticles prepared by a novel method." *Journal of Controlled Release* **2004**, *96*, 245-259.

[96] Lee, K. Y.; Ha, W. S.; Park, W. H. "Blood Compatibility and Biodegradability of Partially N-Acylated Chitosan Derivatives." *Biomaterials* **1995**, *16*, 1211-1216.

[97] Pelletier, S.; Hubert, P.; Lapicque, F.; Payan, E.; Dellacherie, E. "Amphiphilic derivatives of sodium alginate and hyaluronate: synthesis and physico-chemical properties of aqueous dilute solutions." *Carbohydrate Polymers* **2000**, *43*, 343-349.

[98] Yeo, Y.; Basaran, O. A.; Park, K. "A new process for making reservoir-type microcapsules using ink-jet technology and interfacial phase separation." *Journal of Controlled Release* **2003**, *93*, 161-173.

[99] Simon, J.; Kuhner, M.; Ringsdorf, H.; Sackmann, E. "Polymer-Induced Shape Changes and Capping in Giant Liposomes." *Chemistry and Physics of Lipids* **1995**, *76*, 241-258.

[100] Tsafrir, I.; Sagi, D.; Arzi, T.; Guedeau-Boudeville, M. A.; Frette, V.; Kandel, D.; Stavans, J. "Pearling instabilities of membrane tubes with anchored polymers." *Physical Review Letters* **2001**, *86*, 1138-1141.